



BACHELOR THESIS

Deggendorf Institute of Technology
University of Applied Science

Faculty of Applied Natural Sciences and Industrial Engineering
Course of Engineering Physics

Design and Construction of an Infrared Laser Transmitter for a Compact Satellite Laser Ranging System

(Design und Aufbau eines
Infrarot Laser Transmitters für ein
Kompaktes Satellite Laser Ranging System)

Bachelor Thesis in Fulfilment of the Requirements for the Degree
Bachelor of Engineering (B.Eng.)

Submitted by: Pia Lützen, Deggendorf
570309

Supervisor: Prof. Dr. Josef Kölbl

Deggendorf, 06.03.2019

Erklärung

Name d. Studierenden: Pia Lützen

Name d. Betreuers: Prof. Dr. Josef Kölbl

Thema der Bachelorarbeit: Design und Aufbau eines Infrarot Lasertransmitters für ein kompaktes Satellite Laser Ranging System

1. Ich erkläre hiermit, dass ich die Bachelorarbeit selbstständig verfasst, noch nicht anderweitig für Prüfungszwecke vorgelegt, keine anderen als die angegebenen Quellen oder Hilfsmittel benutzt sowie wörtliche und sinngemäße Zitate als solche gekennzeichnet habe.

Deggendorf, den _____ Unterschrift d. Studierenden: _____

2. Ich bin damit einverstanden, dass die von mir angefertigte Bachelorarbeit über die Bibliothek der Hochschule einer breiteren Öffentlichkeit zugänglich gemacht wird.

☐ Ja

☐ Nein

Ich erkläre und stehe dafür ein, dass ich alleiniger Inhaber aller Rechte an der Bachelorarbeit, einschließlich des Verfügungsrechts über Vorlagen an beigelegten Abbildungen, Plänen o.ä., bin und durch deren öffentliche Zugänglichmachung weder Rechte und Ansprüche Dritter noch gesetzliche Bestimmungen verletzt werden.

Deggendorf, den _____ Unterschrift d. Studierenden: _____

Bei Einverständnis des Verfassers mit einer Zugänglichmachung der Bachelorarbeit vom Betreuer auszufüllen:

3. Eine Aufnahme eines Exemplars der Bachelorarbeit in den Bestand der Bibliothek und die Ausleihe des Exemplars wird

☐ befürwortet

☐ nicht befürwortet

Deggendorf, den _____ Unterschrift d. Betreuenden: _____

Abstract

Satellite Laser Ranging (SLR) is in use in different fields, like geodesy and space surveillance. Still, the coverage of SLR-Station around the globe is rather uneven. The demand for more SLR-Stations rises as a broader data base increasing data accuracy and thus improves the correctness of interpretations. However, setting up and running an SLR-Station implies high costs for the leading agencies, which arises from the need for a site for the station, on-site staff and especially high quality instrumentation like high energy laser systems. The technical approach though, enables novel set-up possibilities. Direct drive mounts with high angular velocity allow even fast tracking, a new generation of event-timers enables laser ranging at high repetition rates and small powerful lasers invent new options to place them in the system. The Institute of Technical Physics in Stuttgart exploits these new opportunities by building up a compact Satellite Laser Ranging System, called miniSLR, minimizing overall costs. The complete system should be contained in a 2 m x 2 m x 2 m box which is fully sealed and waterproof. The established laser with a pulse energy of $\sim 170 \mu\text{J}$ is directly mounted onto the telescope mount. Therefore, the whole laser transmitter system is also placed directly on the mount. This limits the size of the transmitter system to a commercial aluminium breadboard of 60 cm x 50 cm. It is equipped with commercial optics and optomechanics, including important controlling and imaging components. A software written by the scientists at the Institute and also already integrated in other SLR systems will be used to control each unit and operate the miniSLR completely autonomously. The concept of the miniSLR has already achieved a paper presented at the "International Astronautical Congress" 2018 in Bremen, Germany. The paper is listed in the References, number [6]. The approach in designing and setting up the system's transmitter is described in this work.

Table of Contents

Abstract	4
List of Figures	7
List of Acronyms	8
1 Introduction to Satellite Laser Ranging	9
2 Theory of Applied Optic Technologies	12
2.1 Satellite Laser Ranging	12
2.2 Integrated Instrumentation	13
2.2.1 Laser Radiation Characteristics	13
2.2.2 Galilean Telescope	15
2.2.3 Thin Optical Layers	16
2.2.4 Power Meter	19
2.2.5 Imaging Sensor	21
2.2.6 Start Signal Detector	21
2.3 Alignment Techniques	23
2.3.1 Shear Plate	23
3 Design Requirements and Implementation	24
3.1 Laser Pulse Source	24
3.2 Beam Shaping Optics	25
3.2.1 Transmitting Telescope	25
3.2.2 Further Beam Expanding Options	28
3.3 Laser Pulse Energy Regulation	30
3.4 Telescope Alignment and Beam Steering	32
3.5 Start Signal for Time of Flight Measurement	33
3.6 Eye Safety Precautions	34
4 Mechanical Issues and Construction Process	35
4.1 Optical Path Implementations	35
4.1.1 Astronomical Mount Set-Up and Dimensions	35
4.1.2 Arrangement of Optical Parts	36
4.2 Gather supporting Optomechanics	37
4.3 Checking and Preparing Equipment	41
4.4 Final System Assembly	41
4.5 Beam Walk Alignment	43
5 Discussion of Further Tasks	44
A Appendix	45
A.1 nLight M30 Data Sheet	45
A.2 Internship Report - Lasercharacterisation nLight M30	47

List of Figures

1.1	Laser Ranging data yield per region. Left: Data on reference frame satellites. Right: Data on GNSS satellites. [6], [9]	9
1.2	Left: current set-up of the miniSLR, showing the laser transmitter on the mount. Right: CAD model of the miniSLR including the planned covers, [6]	10
2.1	Satellite Laser Ranging Principle	12
2.2	Propagation of a Gaussian beam, [13]	13
2.3	Course of power of a pulsed laser	15
2.4	Galilean Telescope, Left: used as magnification telescope, Right: used as beam expander	16
2.5	Constructive interference at an optical thin layer	17
2.6	Beam intensity splitting with a cube	17
2.7	Using a dichroic mirror as beam splitter, [22]	18
2.8	Transmission graphs of selected filters	19
2.9	Absorbance of the integrated thermal power sensor (S401C), [20]	20
2.10	Principle of thermal power sensor, [20]	20
2.11	Simplified depiction of a CMOS-Sensor	21
2.12	Selection of different materials used for photodiodes, [21]	22
2.13	Principle functionality of a Shear Plate	23
2.14	Determination of a beam's divergence with a Shear Plate, [23]	23
3.1	Pulse shape Microlaser M30	24
3.2	Layout of resulting lens combination	26
3.3	Spot Diagram of resulting lens combination	27
3.4	diffraction encircled energy of resulting lens combination	27
3.5	Collimation check of the provided beam expander	28
3.6	Expanded beam and calculated radius	29
3.7	Dimensions of the applied variable beam expander, [19]	30
3.8	Set-up of energy section	32
3.9	Beam steering and object tracking	33
3.10	Start detector responsivity (DET10C2), [21]	34
4.1	Astronomical mount construction	35
4.2	Breadboard dimensions	36
4.3	optical path principle	37
4.4	Tube covers	38
4.5	Variable lens distance, Galilean Telescope	38
4.6	Height flexible mirror mount	39
4.7	Camera fixing	40
4.8	Fixing of variable beam expander	40
4.9	Final set-up of the laser transmitter	42
4.10	Observed pattern on Shear Plate (alignment of lens distance)	43

List of Acronyms

BPP	Beam Parameter Product
CAD	Computer-Aided Design
CCD	Charged Coupled Device
CMOS	Complementary Metal-Oxide Semiconductor
CW	Continuous Wave
DC	Direct Current
DPSS	Diode Pumped Solid State
DYC	Duty Cycle
FWHM	Full Width Half Maximum
GNSS	Global Navigation Satellite System
GPS	Global Positioning System
ILRS	International Laser Ranging Service
InGaAs	Indium Gallium Arsenide
ISS	International Space Station
LEO	Low Earth Orbit
miniSLR	Miniature Satellite Laser Ranging System
Nd:YAG	Neodymium Yttrium Aluminum Garnet
OD	Optical Density
SLR	Satellite Laser Ranging
ToF	Time of Flight
TTL	Transistor-Transistor Logic
UTC	Universal Time Coordinated

1 Introduction to Satellite Laser Ranging

Satellite Laser Ranging (SLR) is an established technology to measure orbits of objects in space by means of a laser [6]. The method is very simple: the Time of Flight (ToF) of a laser pulse to a space object and back to an observer is taken [3], [2]. In the simplest, the distance D to the object is given by $D = \frac{1}{2} \cdot c \cdot ToF$, where c is the speed of light. Compensating atmospheric effects by taking corrections into account, a millimeter accuracy can be reached [4], [2]. The high accuracy qualifies SLR for many different applications, from research in geodesy to scientific mission support [1], [6]. Currently, there are about forty laser ranging stations operating all over the world, whose laser ranging activities are organized under the International Laser Ranging Service (ILRS) [1]. The ILRS collects all generated data from the stations, provides them for research purposes and manages the communication of data providers and users, respectively the SLR stations and researchers [6]. Figure 1.1 shows the distribution of the stations across the globe. Most data is received in the European, Asian and also in the Australian region. However, there is a lack of stations in America, Africa and at high latitudes. One reason to build more SLR-Stations: A more even coverage of them would increase the accuracy of some of the main geodetic data [6]. A further reason might be that there are coming more and more GNSS Satellites that cross-calibrate their positions relying on SLR data. As these data get more precise this process will become more important to the satellite's operators [6]. Another application of SLR is using it as space surveillance tool [6]. Since more space debris fills the orbits around Earth, an awareness of the current space situation is essential. Space debris can be rocket bodies or parts from collisions of (dysfunctional) satellites, like the collision of Iridium 33 and Kosmos 2251 in 2009 which increased the amount of space debris tremendously. The arising parts move at hypervelocity, endangering satellites or even the ISS. Evasive maneuvers have to be executed on a regular basis to avoid collision incidents, in which the false alert rate is far above 99 %. False alerts cause remarkable costs (running an on-call team, planning the manoeuvres etc.). Therefore, a higher quality of orbital data is of great significance to evaluate the need for an evasive maneuver.

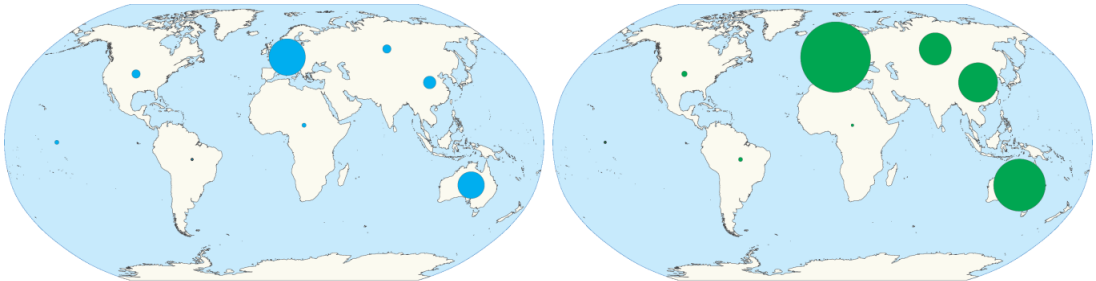


Figure 1.1: Laser Ranging data yield per region. Left: Data on reference frame satellites. Right: Data on GNSS satellites. [6], [9]

Establishing SLR can reduce the alert rate by 1 - 2 orders of magnitude. Deductive, SLR is a promising alternative to solve this problem [7].

However, a retroreflector on every single space object would facilitate and improve the quality of SLR. Ranging to objects without a reflector (uncooperative objects) requires high pulse energies (~ 50 mJ [2]), as only scattered light can be received on Earth. High energy Lasers constitute complete systems, as they need supplies for large cooling and power systems [8]. The low return rate of photons require a larger diameter of the receiving optics [2]. All in one, ranging to uncooperative objects lead to a more complex SLR system set-up. This problem can be solved with a retroreflector, which is easily integrated into a satellite or rocket body, as they are light and small. This method is already successful in use with several microsatellites, e.g. Technosat. The position determination happens with accuracy in the millimeter range [4], [2], trajectories are predicted with uncertainties of a few meters [6]. Summing up, the demand for more SLR stations rises. That's why several stations are built up at the moment. Though, installation and operation of a ground station leads to high costs for the responsible agency, as a site for the station, high energy lasers, sensitive electronics and on-site staff are required. Nevertheless, the technical approach offers new possibilities.

The Institute of Technical Physics at the German Aerospace Center addresses these new opportunities by building up the "miniSLR", a compact SLR Station. For example, a small powerful laser is integrated, which can directly be mounted onto the telescope mount. This eliminates the need for an expensive coudé-path satellite tracking mount. Moreover, direct drive mounts with sufficient tracking accuracy and high angular velocities have become widely available and a new generation of event timers enable laser ranging at high repetition rates. The miniSLR uses a direct drive mount, on which the laser is directly placed. A Newton telescope with an aperture of 20 cm acts as receiver telescope. Electronics and controlling units are contained in an aluminium container. It is sealed and air-conditioned, avoiding possible problems with moisture and strong temperature variations. The miniSLR is designed to be operated fully automated. The controlling

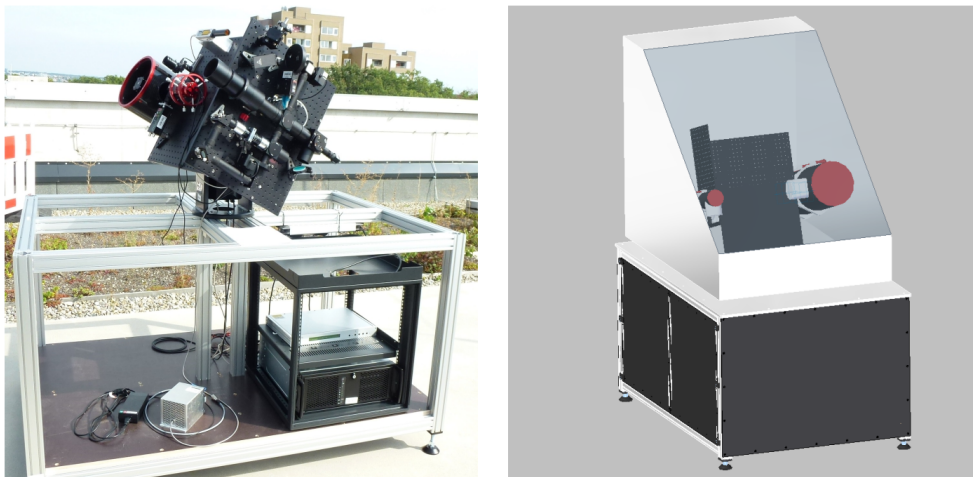


Figure 1.2: Left: current set-up of the miniSLR, showing the laser transmitter on the mount. Right: CAD model of the miniSLR including the planned covers, [6]

software is called OOOS, Orbital Objects Observation Software. It is written by the scientists at the German Aerospace Center in Stuttgart with the main goals of automization and utmost flexibility to use it in many different scenarios [10]: It is employed at already existing SLR stations of the German Aerospace Center Stuttgart, the Uhlandshöhe Forschungsobservatorium ("UFO") and the Surveillance Tracking and Ranging Container ("STAR-C"), an SLR system built into a 20 ft ISO Container. Figure 1.2 shows the current set-up of the miniSLR on the left. A cover for the telescope mount is planned, a CAD model is shown in Figure 1.2 on the right. An important part of the system is the laser transmitter. It shapes the beam (in terms of its diameter) and also has to include an option to correct the outgoing beam's direction to optimize targeting the space object under investigation. Functions have to be controllable with a computer to ensure the automated operation of the miniSLR. The whole transmitter will be mounted onto the astronomical mount, this limits the available area for the optical path and influences its course. This work explains the approach of design and construction of the miniSLR's laser transmitter.

2 Theory of Applied Optic Technologies

This chapter first explains the general principle of SLR followed by further explanations on the transmitter. Instructions to the fundamental functionalities of the integrated optics and analyzing instruments are given to better comprehend why certain components are chosen. Closing, the devoted method to check beam divergences is shortly described.

2.1 Satellite Laser Ranging

In general, a Laser Ranging System includes three parts [11]. The first one is the laser transmitter, which includes a laser pulse source. Moreover, beam shaping optics, beam monitoring sensors and beam steering devices are reasonable to emit feasible laser pulses. After passing all optics as well as measuring and controlling units the beam is led out into space [11]. The photons hit the retroreflector on a satellite and are reflected back to the laser ranging ground station. An optical system collects the reflected photons and leads them onto a detector (e.g. a single-photon detector) in order to capture them. Hence, their ToF is recorded. This forms the second part of a SLR system [11]. The ratio of transmitted and received photons is called the return rate. The third part are controlling and measuring electronics, of which the event timer is the most important. It records the time stamps of emitted pulses and reflected signals and synchronizes with GPS to UTC time (important for satellites)[5]. A computer correlates the time stamps to each other, registers the ToF and calculates the distance to the satellite. The receiver and transmitter telescope are both installed onto an accurate and fast moving mount in order to track space objects. While tracking, a continuous ToF measurement, respectively distance measurement, is done [11] (Figure 2.1).

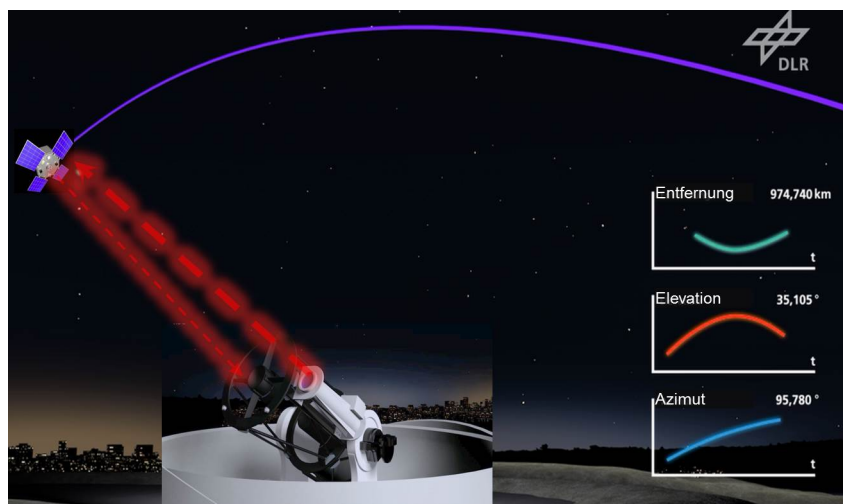


Figure 2.1: Satellite Laser Ranging Principle

2.2 Integrated Instrumentation

2.2.1 Laser Radiation Characteristics

Dealing with laser systems, different characterization parameters occur periodically. This subsection describes the most important ones, concentrating predominantly on pulsed lasers.

The Gaussian Beam

The Gaussian Beam (Figure 2.2) is the most important beam shape in applied laser optics. The name goes back to its gaussian amplitude distribution [13]. The most important parameters are [13]:

- Beam Waist w_0
The beam waist is the radius of the beam's tightest point
- Divergence Angle ϑ (half-angle)
The divergence angle is confined by the z-axis and the asymptotes of the beam profile
- Rayleigh length z_R
At the point of the Rayleigh Length the beam's cross-section area is twice the size as at the beam waist point

The beam diameter $w(z)$ itself is limited to where the beam's intensity accounts $1/e^2$ times the intensity on the z-axis [13].

The Gaussian beam shows the least divergence, therefore it is considered as "ideal case".

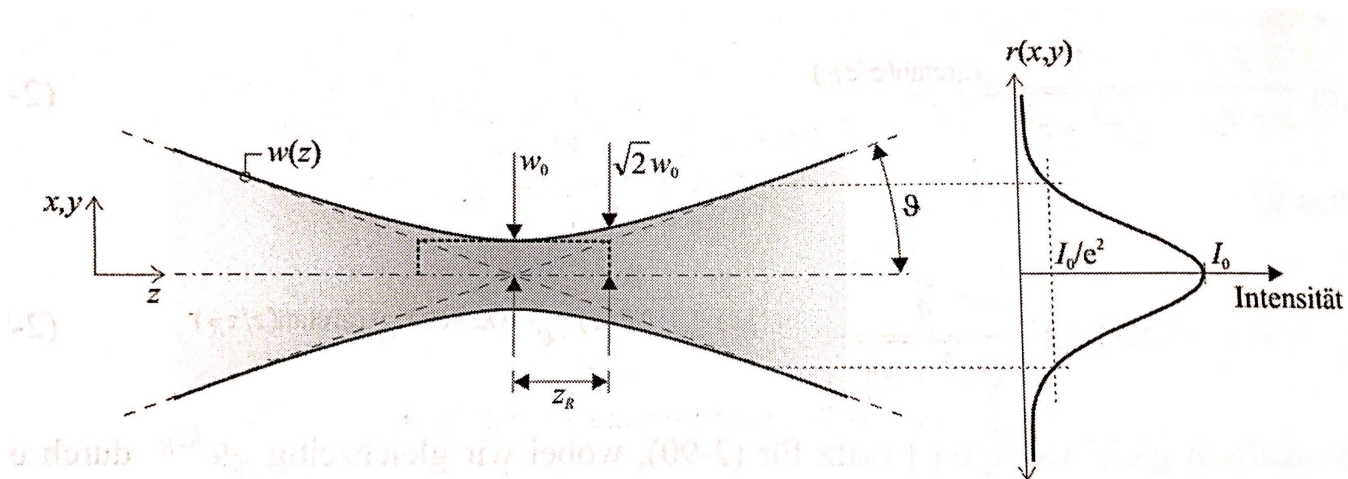


Figure 2.2: Propagation of a Gaussian beam, [13]

In reality though, beam profiles differ from this case [12]. The so-called "Beam Parameter Product" (BPP) describes a beam profile, more precise the focusability. It is constant over the entire extension of the laser beam and depends on ω_0 and ϑ :

$$\text{BPP} = \omega_0 \cdot \vartheta$$

The smaller the value for a beam profile's BPP, the better is the beam's focusability. That means, the beam can be focused to a smaller beam diameter. Nevertheless, diffraction limits this parameter [13]. To scale the BPP to a Gaussian beam, the beam quality factor M^2 is introduced [13]. It is used to generally characterize a beam profile compared to the "ideal case" of a Gaussian beam [12], and is defined as:

$$M^2 = \frac{\pi}{\lambda} \cdot \omega_0 \cdot \vartheta, [13]$$

Interpreting this equation, the beam waist ω_0 and the divergence angle ϑ are increased by the factor M towards the Gaussian beam. The Gaussian beam holds the minimum beam quality factor of $M^2 = 1$, meaning the closer a beam's quality factor is to 1, the "better" or more gaussian-like is the beam. The beam quality factor is a constant over the beam's propagation and hence an appropriate parameter to describe a beam profile [13].

Performance Parameters of Pulsed Lasers

There are different performance parameters for lasers, either for CW- or pulsed laser systems. The following gives an explanation with regard of pulsed lasers and their for understanding typical and important characteristics. All correlations can be illustrated by considering the course of power over time (Figure 2.3). The first fundamental parameter is the pulse width Δt . It corresponds to the temporary duration of one laser pulse. The repetition rate f_{rep} is the amount of pulses in one second, in which its reciprocal is the pulse period T [18]. It is the time of one on/off cycle of the laser [17]. Moreover, in data sheets of pulsed lasers "Peak power" as well as the "Average power" are always documented. The Peak power P_{peak} is the power during the course over one pulse [17]. In figure 2.3 that corresponds to the height of a pulse [18]. In contrast, the Average power P_{avg} is the power averaged over one pulse period [17]. The mathematical relationship can be understood when also considering the energy. Power itself is the amount of energy transferred in one unit of time [17]. Regarding figure 2.3 Energy E is the area under the power line [18]. It can be calculated by multiplying either the Peak power P_{peak} by the pulse width Δt or the Average power P_{avg} by the pulse period T [18]. As the energy is constant in both versions, the areas need to be equivalent. That means:

$$E = P_{peak} \cdot \Delta t = P_{avg} \cdot T, [18]$$

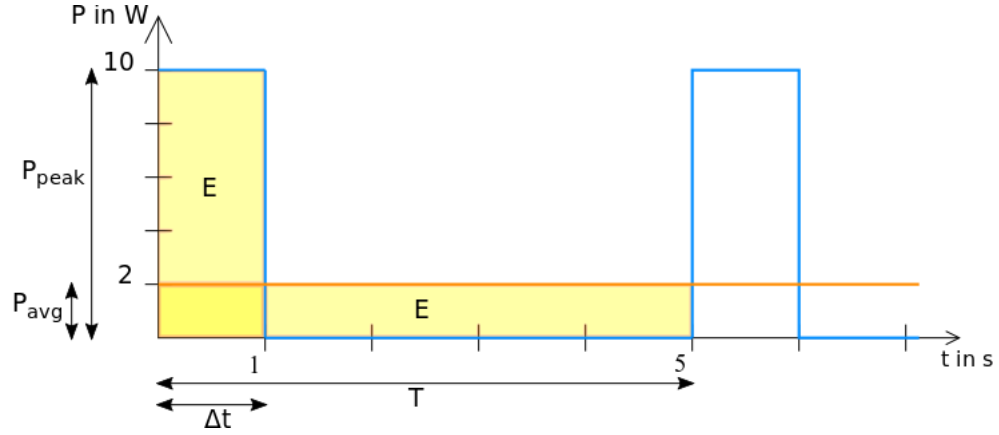


Figure 2.3: Course of power of a pulsed laser

Moreover, there is an additional factor called the Duty Cycle (DYC). It describes the ratio of the pulse width Δt and the pulse period T :

$$\text{DYC} = \frac{\Delta t}{T} = \frac{P_{\text{peak}}}{P_{\text{avg}}}$$

This relationship allows an easy conversion between both forms of power.

2.2.2 Galilean Telescope

The Galilean Telescope is also called a refractor as it uses refractive optical elements (lenses) to focus and collimate light beams [16], in order to see terrestrial or astronomical objects at far distance larger [14]. Objects located at "infinity", meaning far away, deliver parallel bundles of beams. The Galilean Telescope transforms these bundles into, again, a parallel bundle, indeed at an larger viewing angle α' (see Figure 2.4), leading to objects appearing larger. Thus, the effective refractive power equals zero, a property of an afocal system [14]. This is achieved by using two lenses: one convex lens (objective) and one concave lens (ocular). Important is, that the image focal point of the objective coincides with the object focal point of the ocular. The magnification happens in two steps, where the objective generates a virtual intermediate image. This image is observed with the ocular, which is used as simple magnifier [15]. The magnification can be calculated with:

$$\Gamma' = \frac{\|f'_{ob}\|}{\|f_{ok}\|} \left(= \frac{D_{ob}}{D_{ok}} \right), [16]$$

The resulting overall length of the lens constellation, called the mechanical tube length L , of a Galilean Telescope is:

$$L = \|f'_{ob}\| - \|f_{ok}\|, [16]$$

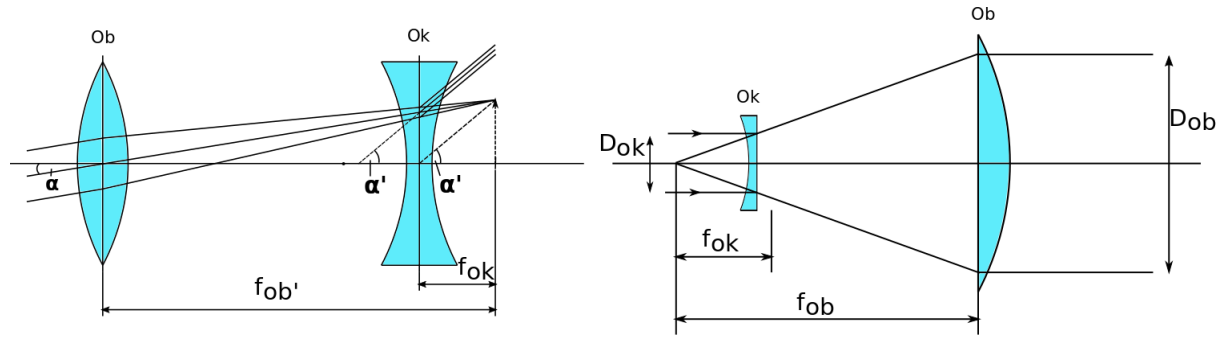


Figure 2.4: Galilean Telescope, Left: used as magnification telescope, Right: used as beam expander

Vice versa, this combination of a concave and convex lens can also be used to expand the diameter of an incident collimated beam, for example a laser beam. The calculation of the magnification and the mechanical tube length stay the same as explained above. Figure 2.4 shows both possibilities to establish a Galilean Telescope.

2.2.3 Thin Optical Layers

Optical interfaces have different reflection- and transmission characteristics, which depend on the refraction index of the two mediums creating the interface. Though, the possible degrees of reflection or transmission depend on the wavelength and polarization of the incident light as they obey the Fresnel'sche equations. Optical thin layers are applied in practice to influence the reflection properties of optical components. Standard are dielectric layers which are transparent in general, however generate two partial reflections at the interfaces (air - layer and layer - air) when illuminated with light with the wavelength λ . With the layer having the right thickness d , constructive interference of the two reflections occurs (figure 2.5), which strengthens the intensity of the superpositioned beams, hence the reflection degree. Constructive interference arises at a layer material with refraction index $n(\lambda)$ when applicable:

$$d = \frac{\lambda}{2n(\lambda)}$$

However, to reach a homogeneous and high reflection degree for a broad wavelength spectrum, so-called multilayersystems are constrained, which exhibit materials of dissimilar thicknesses and refraction indices. [16]

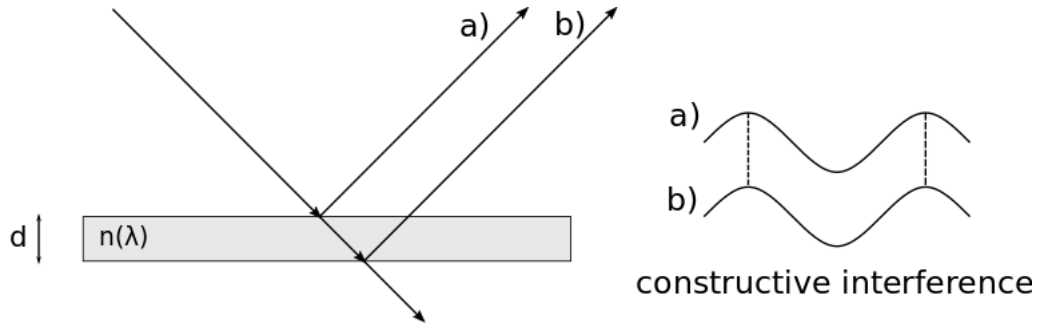


Figure 2.5: Constructive interference at an optical thin layer

Non-Polarizing Beam Splitter Cube

A Non-Polarizing Beam Splitter Cube is compound of two 90°-Prisms, the connecting hypotenuse is coated with a multilayersystem. The effective reflection degree of such a system with two different materials and N layers is given by:

$$R_{eff} = \left(\frac{1 - \left(\frac{n_{M1}}{n_{M2}} \right)^{2 \cdot N}}{1 + \left(\frac{n_{M1}}{n_{M2}} \right)^{2 \cdot N}} \right)$$

Here, n_{M1} and n_{M2} are the refraction indices of the two applied layer materials. Using this equation allows defining a certain ratio of reflection and transmission, hence the intensity of reflected and transmitted light. This way, beams respectively their intensity are splitted into two parts [16] (see figure 2.6).

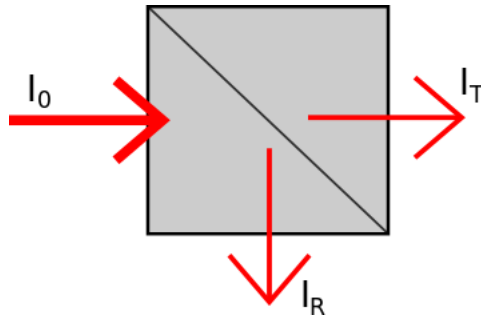


Figure 2.6: Beam intensity splitting with a cube

Reflective Notch Filters

Notch filters are the opposite of interference filters. While interference filters are transparent for a sharp limited wavelength, Notch filters block a selected wavelength (called "center wavelength") and transmit all other ones. This is achieved similar to the multi-layersystems described in 2.2.3, yet more complicated [16]. In general they are "manufactured using the dielectric stack method which involves using a series of thin layers of dielectric materials, of alternating refractive index" [25]. The degree of blocking is defined by Optical Density (OD). Concretely, that is the amount of the beam's energy that is reflected, respectively blocked [24]. A filter that transmits T % of the incident energy, occupies following Optical Density:

$$\text{OD} = -\log\left(\frac{T}{100}\right), [24]$$

A Notch Filter with OD 4 blocking hence transmits 0.1 % of the center wavelength.

Dichroic Mirror

A dichroic mirror transmits and reflects light in dependency of its wavelength [24]. It can be used to split (see figure 2.7) or combine two beams of different wavelengths without a significant loss of intensities [22]. Again, this is achieved by using multiple layers of diverse refraction indices. The different layers cause wavelength-dependent partial reflections or transmission. The reflections interfere purposeful and support reflection or transmission in a pre-selected wavelength spectrum [24]. Here, a dichroit can be a shortpass, transmitting short wavelengths or vice versa a highpass, transmitting long wavelengths [16]. The cut-off wavelength marks the wavelength where transmission turns into reflection and reverse. Figure 2.8 shows the theoretical transmission graph for Notch filters, interference Filters and a shortpass dichroit.

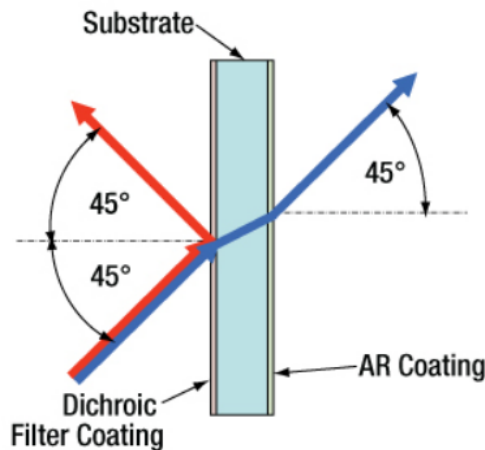


Figure 2.7: Using a dichroic mirror as beam splitter, [22]

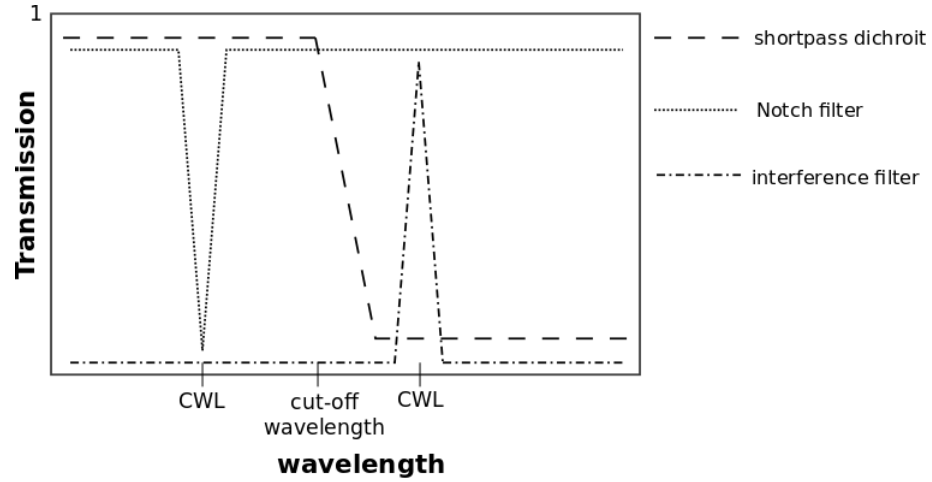


Figure 2.8: Transmission graphs of selected filters

2.2.4 Power Meter

In terms of measuring the average pulse energy propagated through the transmitter, a thermal power sensor is applied. An ideal thermal power detector is a black body. It absorbs all incident light which results in an energy flow. This, in turn, leads to an increasing temperature compared to the environment. The value of this ΔT is measured via a thermopile and subsequently converted into an electrical signal. The probe's temperature change follows this differential equation:

$$\frac{d}{dt} \Delta T = \frac{P_L}{K} - \frac{V}{K} \Delta T$$

where

$P_L \equiv$ Power of the incident Light

$V \equiv$ Heat Loss Rate

$K \equiv$ Heat Capacity

From this equation it can be deduced that the detector integrates the incident light power for short times [14]. Thermal Detectors show a flat spectral dependence over a wide wavelength range [14], which can also be seen in figure 2.9 where the absorbance of the integrated sensor in dependence of the wavelength is plotted.

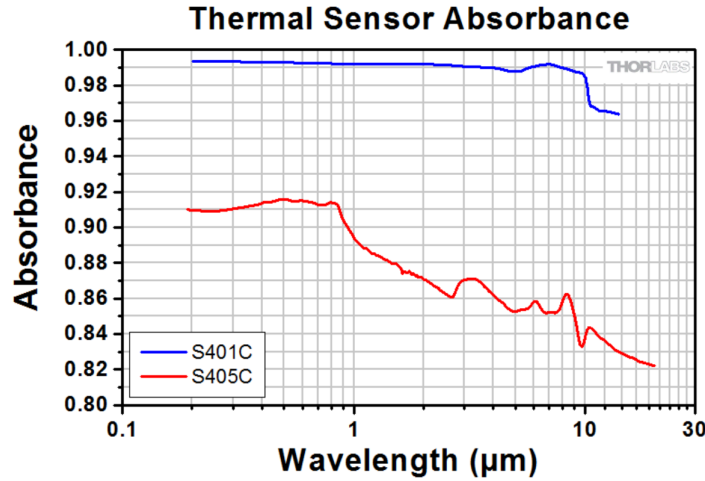


Figure 2.9: Absorbance of the integrated thermal power sensor (S401C), [20]

Moreover, its principle is shown in figure 2.10. The top-layer is the light absorbing layer, a blackened absorber plate. The thickness of the absorbing material determines the maximal optical power detectable by the sensor. In close contact, thermocouples operated in series, are placed. 10 - 100 thermocouples are used, as a single one delivers a very small voltage difference. The lower layer represents a heat sink which is kept at ambient temperature. The voltage of this thermopile is proportional to ΔT , respectively to the power absorbed by the top layer [14], [20]. Due to its integrating character, thermopiles are suited to determine the Average power of pulsed light sources, like the pulsed laser used in this construction.

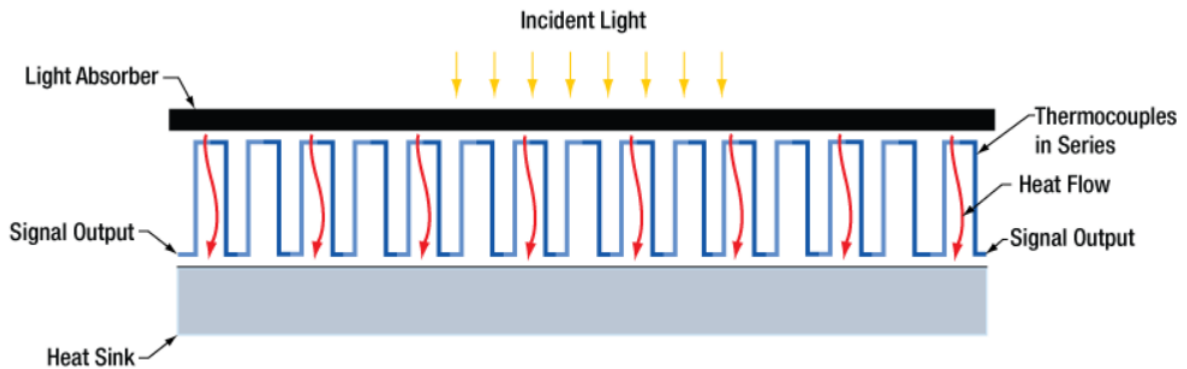


Figure 2.10: Principle of thermal power sensor, [20]

2.2.5 Imaging Sensor

The used Imaging Sensor is a Complementary Metal-Oxide Semiconductor Sensor, abbreviated as CMOS-Sensor, an image sensor integrated for example in cameras to generate digital pictures and analyze them with a computer. It consists, just as a CCD-Sensor, of pixels arranged in a two-dimensional array. The pixels are photoelements in CMOS-Technology which (in case of a monochromatic sensor) measures light intensities and converts them into electrical signals. The sensor is also called Active Pixel Sensor (APS) as each pixel is operated and read out individually. This, however, increases the noise on the one hand, but signal processing gets faster on the other hand [15]. In contrast, the CCD-Sensor processing is more elaborate because it analyzes column per column of the pixel array, though the quality of the signals is much better since it is influenced by less noise. Hence, CMOS-Sensors suit for qualitative analysis and photography but not for quantitative statements in spectroscopy etc. [15]. Still, CMOS-Sensors have a great geometrical resolution, as their pixel edge sizes range from 1 μm to 10 μm [14], which is a perfect precondition for determining object positions within the sensor area regarding the image.

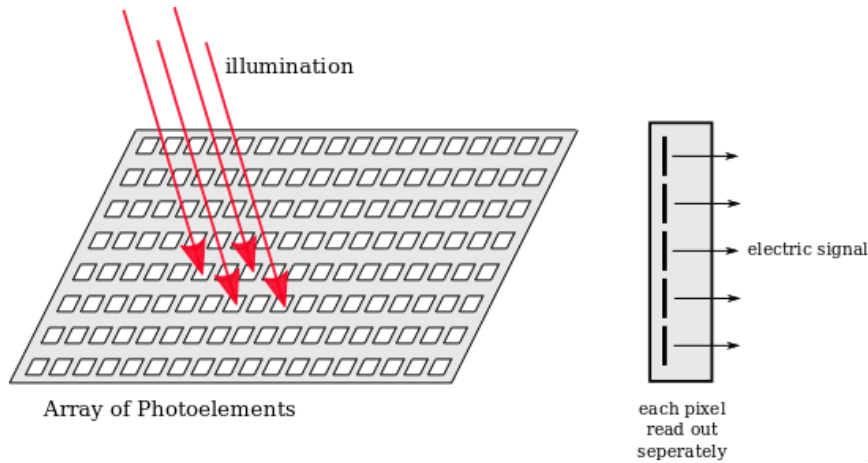


Figure 2.11: Simplified depiction of a CMOS-Sensor

2.2.6 Start Signal Detector

The detector used for the start signal is a Free-Space Biased Detector, precisely a photodiode. A photodiode is an active component which is based on a p-n junction. Illumination of the photodiode leads to an electrical current. The photocurrent is linearly dependent on the absorbed light power [15]. The ratio of the generated photocurrent I_{PD} to the incident light power P is called the "Responsivity" [21], a characteristic of light sensors:

$$R(\lambda) = \frac{I_{PD}}{P}, [21]$$

Another characteristic is the rise time τ . This is the temporal interval during which the photocurrent, in this case, reaches 63 % of its final value when getting a signal respec-

Material	Dark Current	Speed	Spectral Range	Cost
Silicon (Si)	Low	High Speed	Visible to NIR	Low
Germanium (Ge)	High	Low Speed	NIR	Low
Gallium Phosphide (GaP)	Low	High Speed	UV to Visible	Moderate
Indium Gallium Arsenide (InGaAs)	Low	High Speed	NIR	Moderate
Indium Arsenide Antimonide (InAsSb)	High	Low Speed	NIR to MIR	High
Extended Range Indium Gallium Arsenide (InGaAs)	High	High Speed	NIR	High
Mercury Cadmium Telluride (MCT, HgCdTe)	High	Low Speed	NIR to MIR	High

Figure 2.12: Selection of different materials used for photodiodes, [21]

tively when it is illuminated [14]. Photodiodes can be operated at two different modes: photovoltaic mode and photoconductive mode. Whereas the photovoltaic mode is zero biased and exploits the photovoltaic effect, like the photoelements mentioned in 2.2.5, the photoconductive mode is external reverse biased [21]. The width of the depletion region increases which in turn leads to an increasing responsivity. A very linear response is produced, the output current is linearly proportional to the input optical power [21]. Though, the photoconductive mode holds a larger dark current. Dark current is a leakage current, which occurs by applying a bias voltage to a photodiode. It varies with temperature, but also with the material and size of the active area. Hence, the dark current can be limited by choosing a suitable material [21]. Figure 2.12 shows a selection of different materials for photodiodes and their corresponding properties.

2.3 Alignment Techniques

2.3.1 Shear Plate

A Shearing Interferometer is a beam analysis device that helps making a statement about the beam's collimation [23]. In principle, a shear plate splits a laser beam into two parts, both with approximately the same intensity [26]. This is done by a wedged optical plane whose front and back surface reflect the beam [23]. The two reflections are displaced laterally by the thickness of the shear plate which leads to interference in the region where they overlap [26] (see figure 2.13). This region is made visible by a diffuser plate with a reference line down the middle [23]. The pattern on the diffuser plate contains information about the beam's collimation, as the fringe rotation of the interferogram relative to the reference line is investigated [26]. Figure 2.14 shows the possible patterns. With the fringes rotated clockwise the beam is converging, a counterclockwise rotation indicates a diverging beam, and as the fringes are parallel to the reference line, the beam is collimated. However, the fringes are also sensitive to spherical aberration, coma and astigmatism [23].

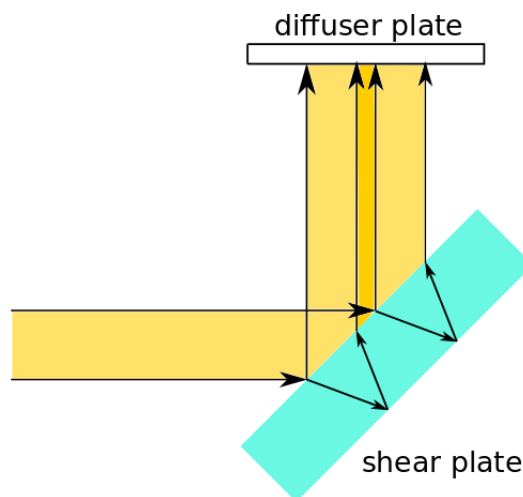


Figure 2.13: Principle functionality of a Shear Plate

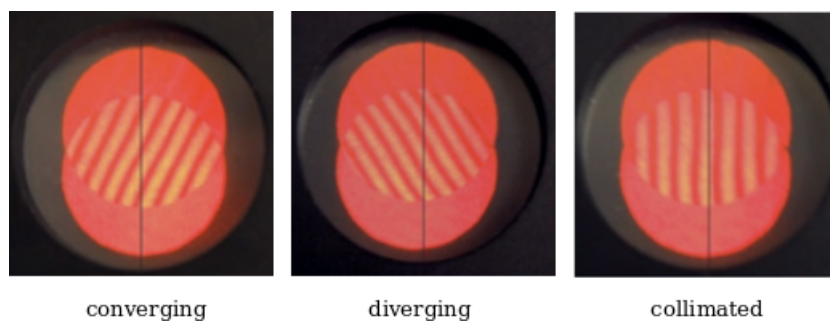


Figure 2.14: Determination of a beam's divergence with a Shear Plate, [23]

3 Design Requirements and Implementation

For the laser transmitter there are given requirements which functions it should include. As the beam-shaping unit there have to be beam expanding optics as well as the possibility to control and measure the energy of the laser pulses. Furthermore, there is a need to get a start signal for the ToF measurement, a way to steer the beam and to see its target. The following explains and justifies the requirements and their realizations. All functional principles, correlations and referenced parameters are explained in section 2.2.

3.1 Laser Pulse Source

The laser in used is acquired from the manufacturer nLight and is called the Microlaser M30. It is a passively Q-switched DPSS random polarized Nd:YAG-laser with an operating wavelength of 1064 nm. Therefore, it is in the near-infrared regime and not visible to the human eye. When emitting laser pulses from the ground into the atmosphere pilots in aeroplanes are not blinded this way (Still, direct eye contact is dangerous due to relative high pulse energies). The laser's beam quality factor M^2 is measured to 1.1 with a pulse width of 4.3 ns (FWHM), see figure 3.1. The procedure of the Measurement and other specifications can be found in appendix A.2. The beam diameter ($1/e^2$) is ~ 0.4 mm. According to the data sheet, the Peak power comes to approximately 38 kW, hence making the laser pulse energy sufficient for laser ranging to Low Earth Orbit (LEO).

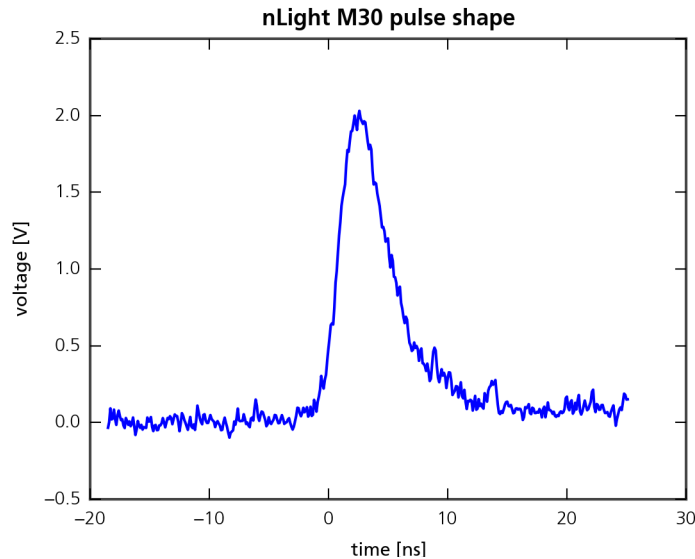


Figure 3.1: Pulse shape Microlaser M30

Still, the laser is very light and handy, matching perfectly the requirements for a compact SLR system and allowing to mount the laser head onto the astronomical mount. A pulse generator provides a TTL signal, necessary for triggering the short laser pulses, resulting in a pulse repetition frequency of 29 kHz. The pulse generator is connected to a laser driver. Both, however, can be installed in the bottom housing, as an optical fibre leads the signal from the driver to the laser head on the mount. The laser's complete data sheet can be found in appendix A.1.

3.2 Beam Shaping Optics

Due to large distances between the SLR ground station and the satellites ($\sim 800 - 2000$ km) a large beam diameter and minimal divergence are essential to hit the retroreflectors and thus achieve high return rates. Moreover, the beam's energy density is reduced with a larger diameter and eye safety is improved. There were several possibilities to magnify the beam's diameter.

The beam is expanded in more than one step, as a very large magnification factor (from 0.4 mm to 50 mm) is necessary.

However, one of the expansion steps is obligatory performed by the transmitter telescope, being the last expansion and the last unit the laser pulse passes by. The output aperture diameter will range around 75 mm. This is the best compromise between the transmitter's physical length, weight and costs. For best use of this aperture, the beam diameter should be about $\frac{2}{3}$ of the last lens. These are 50 mm, in which a real beam diameter between 50 mm and 60 mm is acceptable.

Further given options are two variable beam expanders, one motorized and controllable with a software, the other one needs to be adjusted manually. Both have a possible magnification factor of 2 - 8. Moreover, there is an expanding and collimating optic provided with the laser with a theoretical expansion factor of 20. It simply can be screwed to the laser output aperture. The selection of the final integrated expanders is explained in the following.

3.2.1 Transmitting Telescope

With these initial information the first task is to determine the best lens constellation for the transmitter telescope. For this purpose the simulation software "Zemax - Optical Studio" is used, where several lenses from the manufacturers Edmund Optics and Thorlabs are investigated. Both suppliers offer Zemax files with every optic component, including all important optical properties. The files can be downloaded and easily inserted in a Zemax simulation. It was decided to build a simple Galilean Telescope as expander. It generates a virtual intermediate image, avoiding a real focus causing a large energy density because of the laser pulse's high energies. Different lens combinations are simulated. There are three parameters forming the general conditions. First, the output diameter has to fit the last lens as explained above (output beam diameter of 50 mm - 60 mm). Second, a suitable magnification has to be achieved. The magnification does not have to have a concrete value. Still, it has to be large enough, so that the other expanders are sufficient for the entire magnification of the beam to reach the targeted output beam diameter. Third, and most important, is a minimum divergence. As already explained above, the

distance from the ground station to LEO-Objects is significantly large and a divergent beam would lead to too few photons hitting the satellite's reflectors. Moreover, the length of the lens combination has to be taken into account, since it has to fit the size of the breadboard.

Starting the simulation in Zemax, first general parameters have to be set. The Aperture Type is set to "Entrance Pupil Diameter", which is the diameter of the pupil as seen from object space. The aperture value (corresponding the input beam diameter) depends on the magnification factor of the current lens combination. The goal is an output beam diameter of 50 mm - 60 mm. A tick is set to "Afocal Image Space" to investigate the beam's properties in divergence dimensions. Furthermore, the wavelength is set to the laser's wavelength of, in Zemax units, 1.064 μm . The simulation is done in Zemax' sequential mode, which means that imaging systems are described by sequential optical surfaces: Each ray hits every surface once in a predetermined sequence (in contrast to non-sequential mode where not every surface has to be hit necessarily).

The next step is to insert the first lens combination with an appropriate magnification factor. The necessary input beam diameter has to be achievable with the remaining expanding options. The aperture value is set to fulfill the criterion mentioned above. By means of Zemax' optimization tool the distance between the two lenses is optimized with regard to a minimum divergence. Then the resulting spot diagram is analyzed, which displays the divergence in mr. The layout shows the set-up of the lens combination and spatial dimensions can be measured. In addition, the diagram of the diffraction encircled energy indicates possible energy loss caused by diffraction effects. This way, various combinations are investigated until finding the best solution.

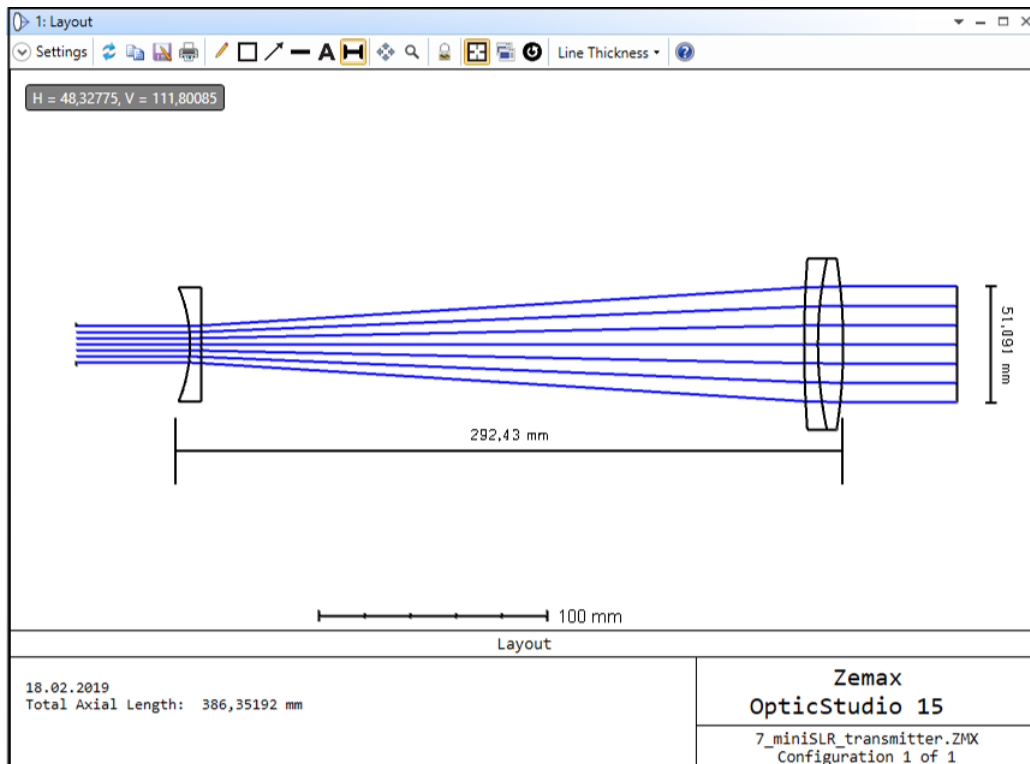


Figure 3.2: Layout of resulting lens combination

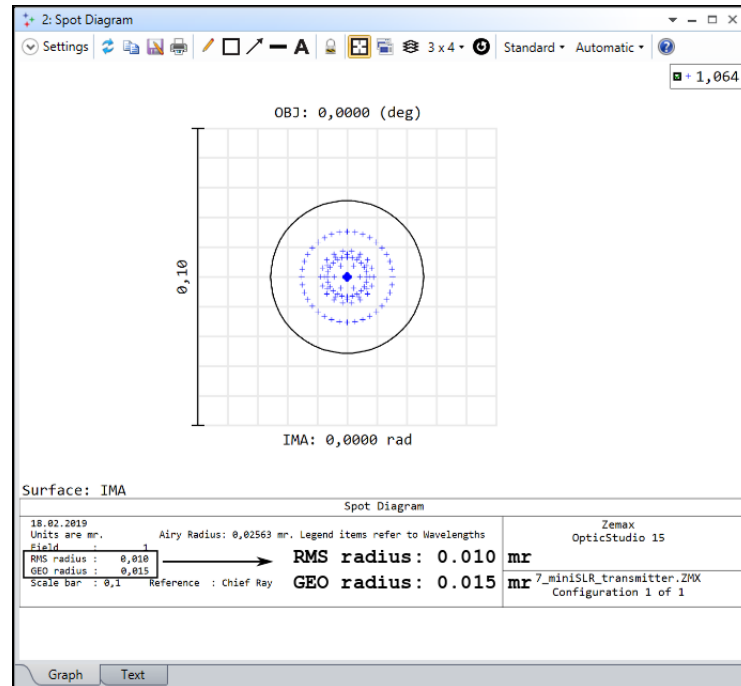


Figure 3.3: Spot Diagram of resulting lens combination

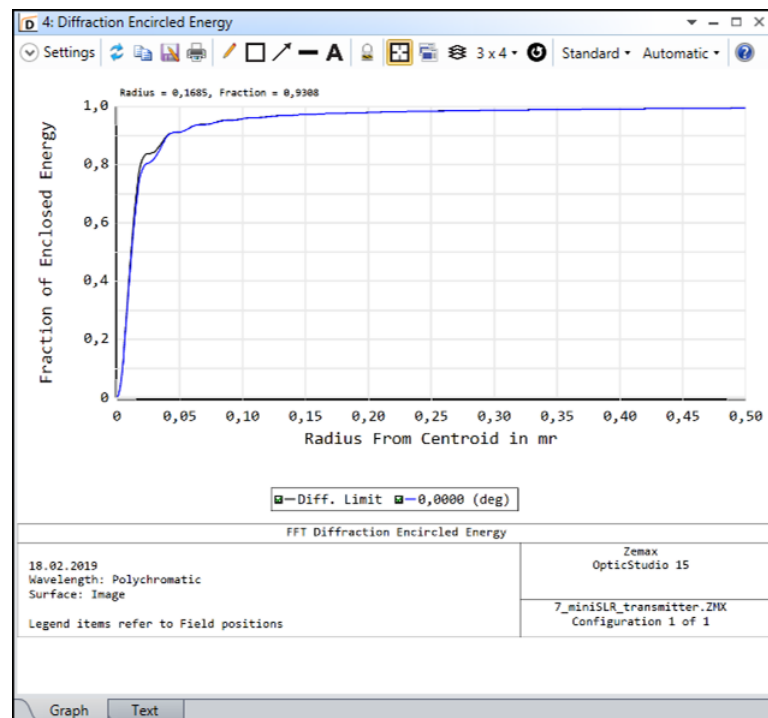


Figure 3.4: diffraction encircled energy of resulting lens combination

The solution is a combination of a plano-concave lens with a focal length of -125 mm (Edmund Optics - item no. 68-004). Its diameter is 50 mm. The second part is an Achromat, 75 mm in diameter (Edmund Optics - item no. 88-598). The focal length is 400 mm. The lenses utilize thin film coatings that minimize reflections for a wavelength of 1064 nm. Considering 3.3, the divergence comes to 0.010 mr, which is the best achieved value. The constellation is approximately 300 mm in length and the resulting beam diameter is approximately 50 mm (see 3.2). Additionally, there is almost no energy loss, the encircled energy corresponds nearly to the diffraction limit, figure 3.4. This combination results in a magnification factor of 3.2. Therefore, the input diameter is set to 16 mm. That means the remaining expanding options need to magnify the beam from 0.4 mm to ~ 16 mm diameter, which corresponds an overall magnification of 40.

3.2.2 Further Beam Expanding Options

The first picked expander is the one provided by nLight with its laser M30. One advantage is that it easily can be screwed onto the output aperture of the laser, saving valuable and limited space on the astronomical mount. Another main advantage is its collimating property, which eliminates the need for an additional collimation lens. Furthermore, it reduces the risk of false alignment of the separate lens. Hence, the optical add-on is further investigated. First, its collimation is checked with a shear plate. The experimental set-up is shown in figure 3.5.

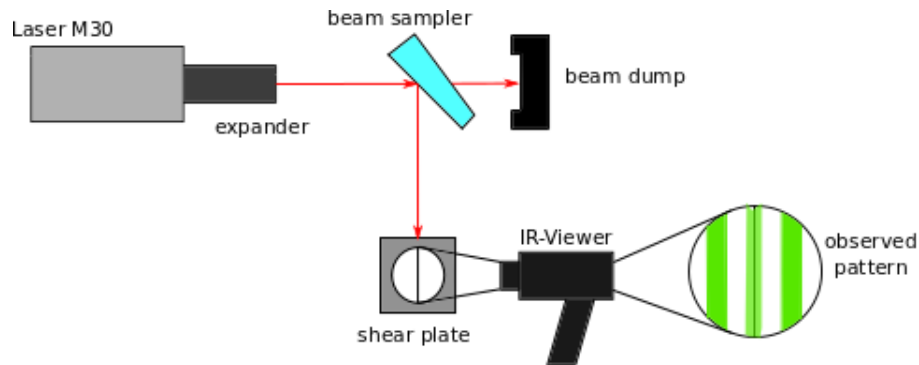


Figure 3.5: Collimation check of the provided beam expander

A beam sampler reflects about 4 % of the pulse energy to protect the shear plate. The scattering on the shear plate's diffuser plate is visible with an infrared-viewer, and a perfect collimation pattern can be observed. However, the beam diameter behind the expander is important, to know if the remaining available expanders suffice for the transmitter's entire magnification. Therefore, a picture of the beam is taken and a self-written python script calculates the beam's radius ($1/e^2$) by means of image processing methods. The radius comes to about 2.1 mm corresponding a diameter of 4.2 mm (see figure 3.6).



Figure 3.6: Expanded beam and calculated radius

With a magnification of the transmitter telescope of 3.2, the remaining expansion has to range between 3.7 and 4.5:

$$4.2 \text{ mm} \cdot 3.2 = 13.4 \text{ mm}$$

lower magnification limit (beam diameter of 50 mm):

$$\frac{50 \text{ mm}}{13.4 \text{ mm}} = \mathbf{3.7}$$

upper magnification limit (beam diameter of 60 mm):

$$\frac{60 \text{ mm}}{13.4 \text{ mm}} = \mathbf{4.5}$$

Hence, one of the remaining expanders is sufficient for the last expansion. As these are perfect preconditions for the whole system, the add-on is chosen for one of the expansion steps.

For a third expansion step it has to be decided if using the motorized beam expander or the manual adjustable one. The advantage of the motorized beam expander is clear: the beam diameter can always be varied via a software. Nevertheless, this is no urgent must-have for the transmitter, the beam just has to eventually have a diameter between 50 mm and 60 mm. Furthermore, the expander is very bulky and heavy in comparison to the manual expander. Although the manual expander can not be changed remotely, it is handy and light (see figure 3.7 for dimensions). The whole transmitter will be mounted on the astronomical mount, so the weight criterion predominates. Therefore, the manual variable beam expander (QI Optiq - item no. 4401-256-000-20) is picked for the transmitter system.

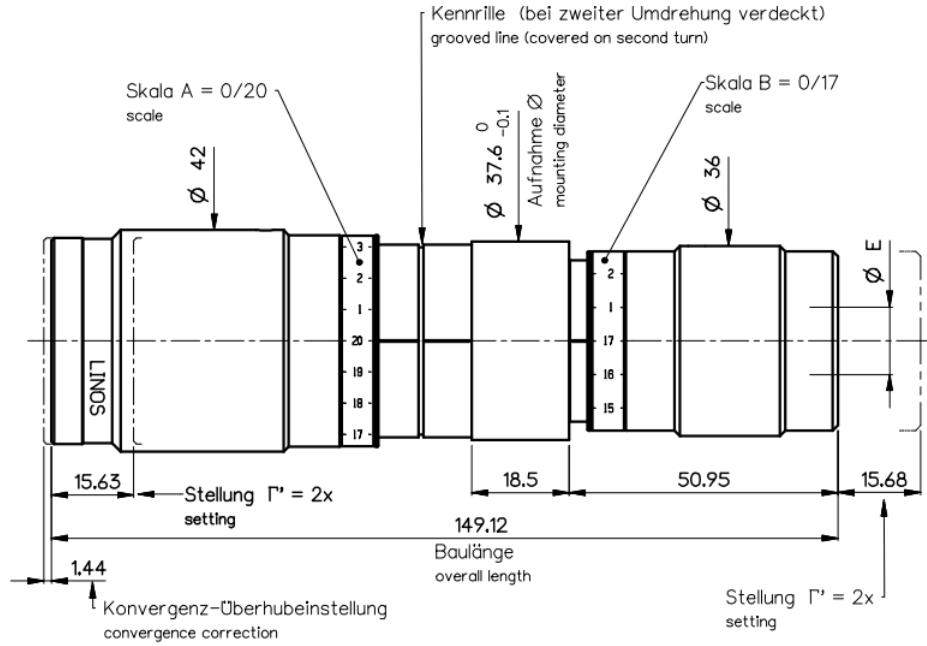


Figure 3.7: Dimensions of the applied variable beam expander, [19]

3.3 Laser Pulse Energy Regulation

The Laser Pulse Energy Section controls and measures the energy of the emitted pulses. Both units are accessible via a computer. For deciding how to control the energy, it is important to know that there is only a need for countable states of energy: for adjusting the transmitter (very low energy), for first calibration measurements (low energy) and eventually for the real ranging measurements (full energy). An included energy screening part is essential to always monitor the real temporary transmitted pulse energy. The section set-up is shown in figure 3.8.

There are several possible ways to control the energy of a laser pulse. For example, a combination of a half-wave plate and a polarizing beam splitter cube would allow a continuous variable setting. Yet, a half-wave plate can only process linear polarized light. The used laser, though, is randomly polarized, causing no reproducible states by the rotatable half-wave plates. An extra optic component like a birefringent crystal would be needed to first filter out one polarization state. This moderates the pulse's energy additionally. Furthermore, a continuous variable setting is an unnecessary feature as explained above. Therefore, it is decided to use reflective Notch filters. They fit into a common motorized filter wheel (Thorlabs - item no. FW102C) which was already available and did not have to be bought newly. It can mount six filters with a diameter of 1 in. The filter wheel can be connected to a computer and operated remotely. Another advantage is that the filters reflect the blocked energy, resulting in a higher damage threshold than for example Neutral Density (ND) Filters. ND-Filter act absorptive and are way more sensitive, not sufficing for the pulse energy of the used laser. The available moderation factors for the operating wavelength are OD 4 (Edmund Optics - item no. 67-123) and OD 6 (Edmund Optics - item no. 86-128), which matches the requirements for three

countable energy states.

In order to monitor the energy after attenuation, a power meter (Thorlabs - item no. S401C) is inserted (see 2.2.1 for correlation between energy and power). Thermal power meters are smaller and way more compact than other energy sensors, hence fit perfectly in the compact transmitter system. As the sensor would block the optical path, a beam splitter cube is applied, exhibiting a reflection-transmission Ratio of 90:10 (Thorlabs - item no. BS029). The cube transmits 10 % of the energy onto the sensor, achieving the smallest possible moderation of the laser pulses. The remaining 90 % are reflected. This property is used to again save space on the available plane, as no additional mirror has to be used. This method, however, requires a very sensitive energy sensor. The picked sensor is a high resolution thermal power sensor from Thorlabs. It can detect optical powers ranging between 10 μW and 1 W. There are three energy states that have to be investigated: blocking with OD 4 and OD 6 and no blocking. The power sensor always absorbs 10 % of the set energy. Following calculation checks the power, that has to be detectable with OD 4 blocking.

Percentage of the Average power transmitted by the Notch Filter:

$$\begin{aligned} T &= 10^{-\text{OD}} \cdot 100 \\ &= 10^{-4} \cdot 100 \\ &= 0.01 \% \end{aligned}$$

Percentage in Watts at the beam splitter:

$$\begin{aligned} P_1 &= 0.01 \% \cdot 5.6 \text{ W} \\ &= 560 \mu\text{W} \end{aligned}$$

Fraction transmitted by the beam splitter onto the power sensor:

$$\begin{aligned} P_2 &= 10 \% \cdot 560 \mu\text{W} \\ &= 56 \mu\text{W} \end{aligned}$$

This value is within the sensor's optical power range. Performing a similar calculation without OD Blocking for the operation without any energy moderation, the result comes to 0.56 W to detect which is also in the limit of the picked laser. However, considering the highest attenuation of OD 6 in the filter wheel, the calculation results in only 0.56 μW to detect. It is very hard to find a sensor which fulfills these sensitivity requirements. However, this energy state is only envisaged for the alignment procedure, not in operation. Hence, it is acceptable to not be able to measure the correct energy while blocking the beam with an OD 6 Notch Filter.

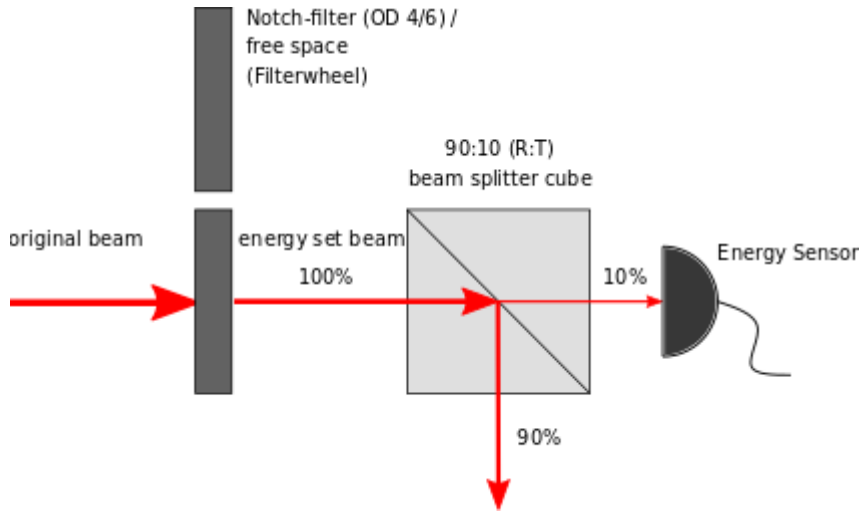


Figure 3.8: Set-up of energy section

3.4 Telescope Alignment and Beam Steering

The main object tracking is carried out by the receiver telescope, still a transmitter pointing model is implemented to encounter systematic misalignment between the transmitter's and receiver's optical axes. Also a closed loop tracking is possible: The off-set in the image of the object under observation to the target point (near image center) is used to correct the pre-programmed trajectory. Moving the object to the beam's target point increases the return rate of photons while ranging. Additionally, the beam's direction should be controllable to iteratively adapt the beam's target and maximize the return rate. Therefore, a beam steering possibility is built in. This is realized whilst mounting the last mirror into a kinematic mirror mount (Thorlabs - item no. KM200). The tip/tilt screws can be controlled with motorized DC Actuators (Thorlabs - item no. Z806), which are driven by a matching controller connected to a computer. The actuators have a travel length of 6 mm and a minimum achievable incremental movement of 0.05 μm . Thus, the beam can be deflected by about 54 mrad with an accuracy of 0.4 μm . A subsequent shortpass dichroic mirror (Thorlabs - item no. DMSP805L) with a cut-off wavelength of 805 nm reflects the IR-beam into the transmitter telescope.

In addition, a passive optical part is required to support the pointing model. A camera (FLIR - item no. BFLY-U3-23S6M-C) with a CMOS Imaging-Sensor, monochrome, is placed behind the telescope and the dichroic mirror, which transmits the visible light (see figure 3.9). With a plano-concave lens the sensor is focused to infinity to detect orbital targets. On the one hand, systematic displacements between transmitter and receiver can be corrected. On the other hand, the beam's direction can be adapted via the actuators. To this, the positions of the actuators have to be calibrated to the camera's sensor coordinates. A retroreflector is temporarily placed directly in front of the transmitter telescope. The dichroic mirror transmits 0.5 % in the IR-Regime which suffices for the large intensity of the incident light. The beam can be seen on the camera and the actuator's positions can be compared to the beam's coordinates on the camera sensor. The camera's sensor is a monochromatic CMOS-Sensor with 2.3 Megapixels. Each pixel has a size of 5.86 μm .

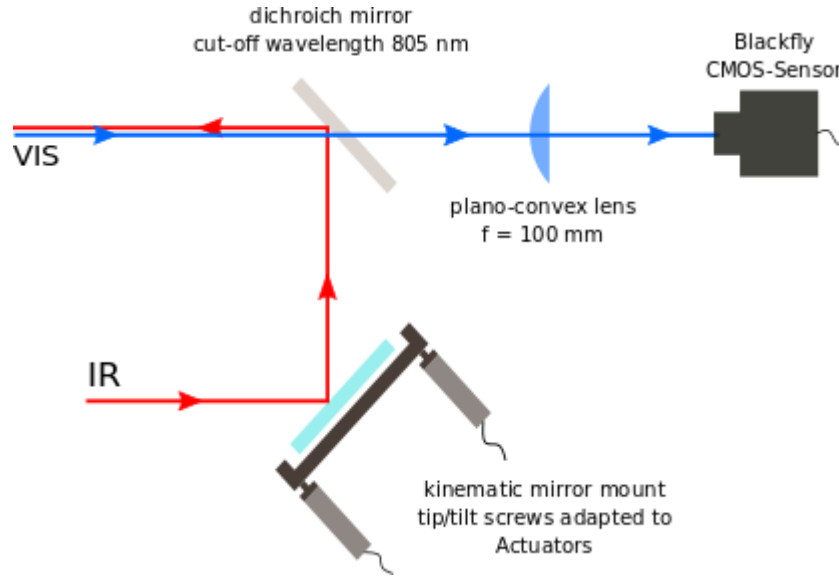


Figure 3.9: Beam steering and object tracking

These specifications suit to determine the beam's position on the sensor very accurate which increases the calibration and pointingmodel quality. Leaving out the reflector, the camera is also used to investigate the orientation of the transmitter telescope relative to the tracking telescope by comparing both fields of view. The beam steering possibility is important for the best possible orientation alignment of the whole system.

3.5 Start Signal for Time of Flight Measurement

For the ToF measurement the event timer has to get a signal when the pulse is emitted. This is done with a Biased InGaAs Detector with a rise time of 10 ns (Thorlabs - item no. DET10C/M). This, indeed, causes signal blurring as the pulse length is shorter and results in a systematic offset. However, this offset is taken into account during the calibration process [5]. The diode is operated in photoconductive mode, increasing its responsivity. Figure 3.10 shows the responsivity of the detector (DET10C2). Considering figure 2.12, the InGaAs Detector is a good choice to eliminate dark current at appropriate costs. However, the rise time represents 10 ns, which is fast enough for the measurement. Concerning the detector's position in the transmitter, the signal has to be picked up before the pulse is manipulated, otherwise the time response of the diode is changed and the measurement would be distorted. As the excitation of intrinsic photoelectrons often needs a much lower energy (photoconductive mode) [14], a scattered light fraction of the first mirror is sufficient as start signal.

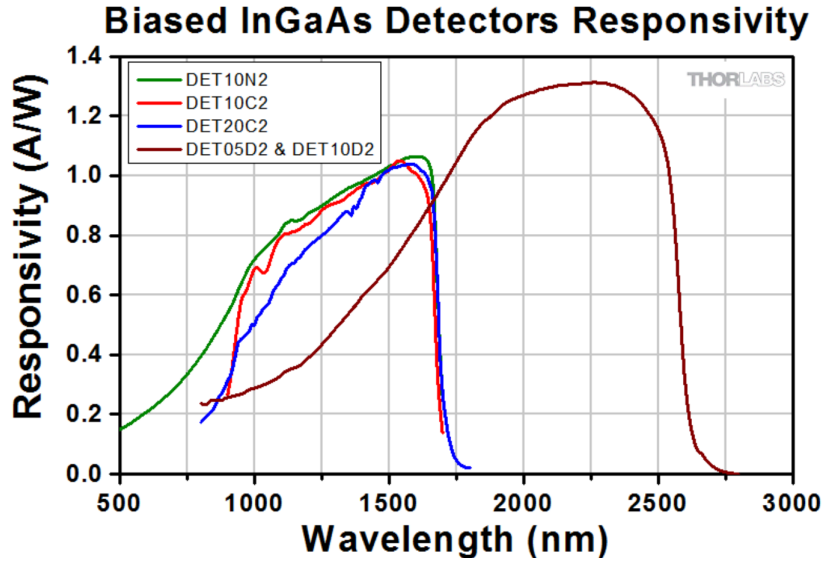


Figure 3.10: Start detector responsivity (DET10C2), [21]

3.6 Eye Safety Precautions

As the used laser is dangerous to the human eye, it was investigated how to isolate the light pulses and scattering. The first and simplest answer was a laser-safe cover above the whole construction. However, it was decided to build all components into tube constructions, since most components and their mounts are compatible with 1"/2" internal/external threads. This facilitates the beam walk adjustment and stabilizes the component's positions to each other at once. However, further adaptations are required. The filter wheel has to be built in a little angle to the optical axis, to steer the reflections of the Notch filters into a beam dump. The moveable mirror's mount has to be optimized, no kinematic mount was found which can be controlled by actuators and simultaneously be implemented into a tube system. Nevertheless, the rest of the optical path runs inside these tubes. Moreover, an optical shutter (Thorlabs - item no. SH1) is built into the optical path. This allows to be able to interrupt the laser emission instantly at any time while operating the system. It is also connected to a controller which is steered with a software.

4 Mechanical Issues and Construction Process

4.1 Optical Path Implementations

4.1.1 Astronomical Mount Set-Up and Dimensions

For mounting the optical set-up of the miniSLR, two solid aluminium breadboards are used. They allow a simple and flexible attachment of all optics as the breadboards have M6 threads on 25 mm centers like common optical tables. The two boards are screwed together in a right angle with a little overlap. Two boards are effectively separating receiver channel and transmitter channel, creating the necessary space for all components. However, due to space-saving reasons, the laser with its collimating and expanding add-on is placed on the board for the receiver channel, which needs way space than the transmitter channel. figure 4.1 shows the construction of the astronomical mount.

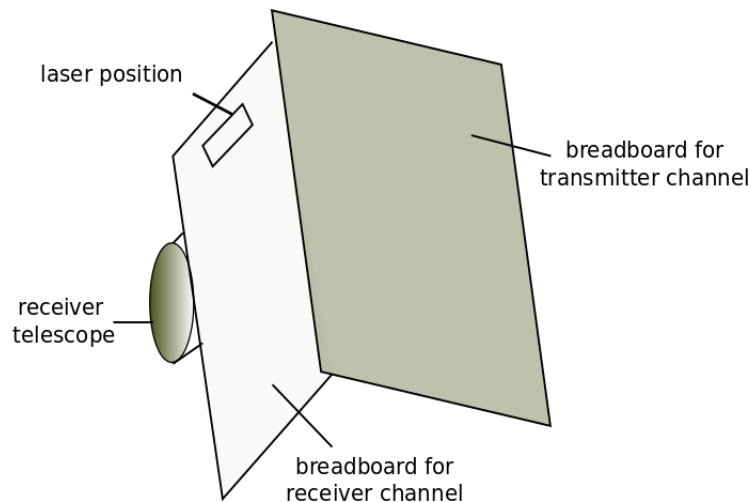


Figure 4.1: Astronomical mount construction

The dimensions of the breadboard for the transmitter are about 60 cm x 50 cm. In the beginning of the construction it was not clear if there is a need for stabilizing the mount's position due to the transmitter's weight distribution. Hence, two weights are selected and their positions are determined, so a planning of the optical path is possible. The resulting still usable space is shown in figure 4.2, in which the dashed lines delimit the space at the edges of the board reserved for the weights.

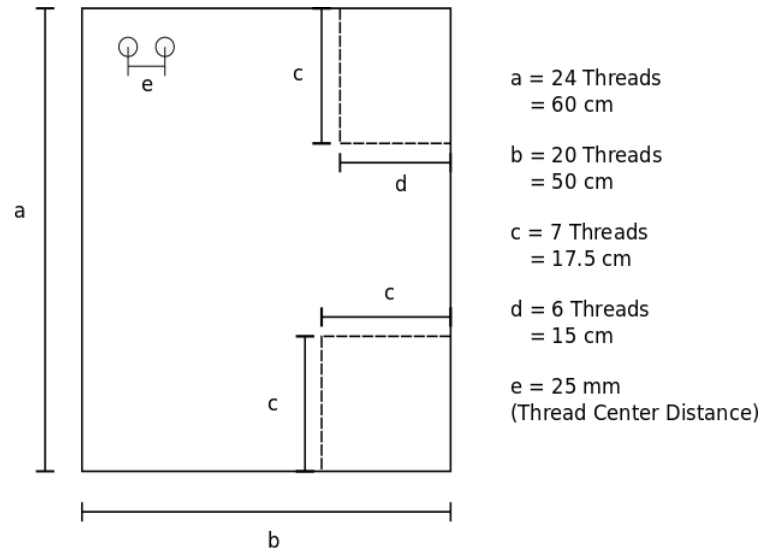


Figure 4.2: Breadboard dimensions

4.1.2 Arrangement of Optical Parts

For a better overview the following list shows again the components to be inserted:

- Galilean Telescope
- Variable beam expander
- Energy regulation
- Beam steering
- Start Signal

The first position determination concerns the output aperture, corresponding the Galilean Telescope's last lens, which has to be placed roughly centered of the breadboard's longer side, so it is orientated equally to the receiver telescope. Moreover, comparing figure 3.2 to figure 4.2, the Galilean Telescope needs $\sim 30 \text{ cm}$ plus a mirror which directs the beam into the telescope optics. Therefore, the centered placement is the only option making sense. In front of it, the beam steering and object tracking unit is placed. As explained in subsection 3.4, this unit needs to be placed right before the transmitting telescope. Furthermore, the included mirror should be the last one, otherwise the steering process would be affected by more adjustment errors and would unnecessarily be complicated. The position of the variable beam expander is results out of its magnification. Since the beam diameter increases significantly, the subsequent optics have to have a diameter twice as large as in front of the expander. To save costs, the expander is placed before the moveable mirror. Hence, only the dichroic mirror, the moveable mirror and the plano-concave lens have to be bought in larger dimensions. Concerning the energy section, the reflecting property of the beam splitter cube is used. The cube is placed at an edge of the optical path, so no additional mirror has to be built in taking up more space of the breadboard. To combine energy setting and screening, the upper left edge

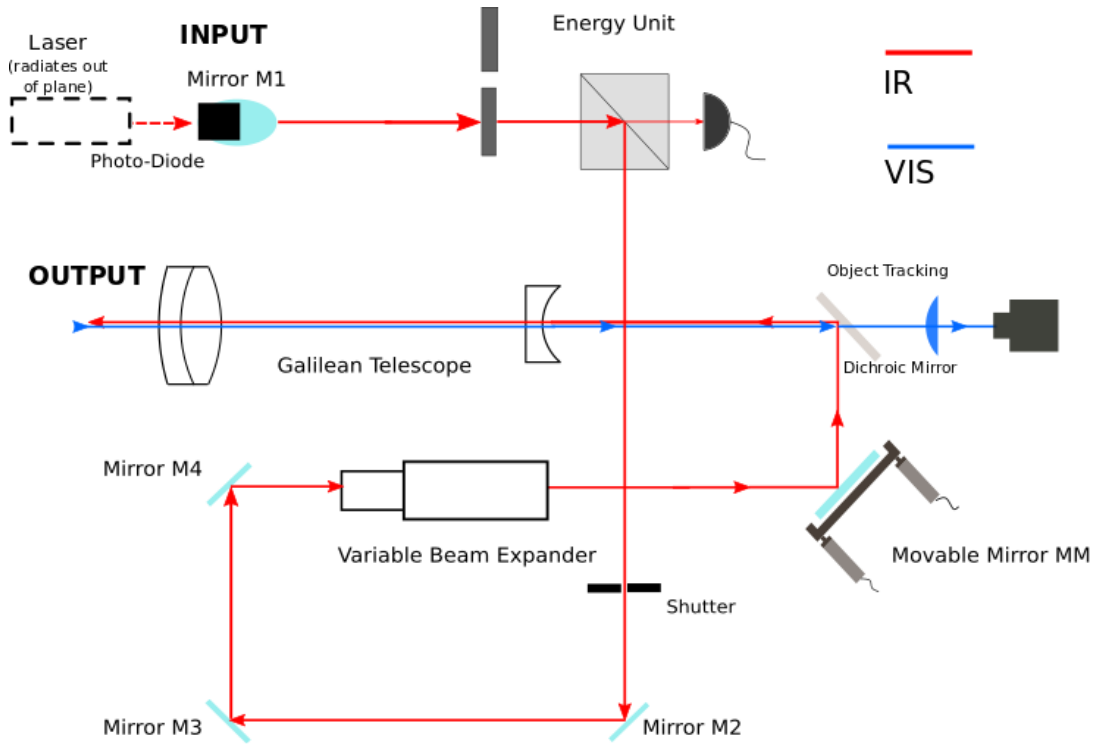


Figure 4.3: optical path principle

is chosen, where the filter wheel fits in front of the beam splitter cube. As mentioned in subsection 3.5, the photodiode is placed behind the back surface of the first mirror, using a scattered, yet not influenced light fraction. The shutter has an aperture of 1 in, so it has to be placed somewhere in the optical path where the beam's diameter is still small enough and the space is available. The optical path in principle is shown in figure 4.3.

4.2 Gather supporting Optomechanics

After determining the transmitter's components and their arrangement the necessary optomechanics have to be found. Apart from the dichroic mirror, all optics were already available in the laboratory. At this point, the breadboard is not mounted onto the telescope mount yet, which allows quick construction and design changes. The optics are attached to the breadboard as planned. This enables to easily see which mechanics are still missing, for example some optic mounts which are compatible with tube constructions. Additionally, the transmitter includes 1 in, 2 in and 3 in optics, therefore some adapters and connecting pieces have to be purchased. Moreover, a first conceptional build-up shows the distances between the optics and the necessary length of the tube covers (see below) can be estimated roughly. These are the basic required optomechanics. However, while searching for them, some construction problems occurred. How they are solved and which additional mechanics are required is explained in the following paragraphs.

Tube Covers Thorlabs offers anodized aluminium tube covers, which come in lengths of for example about 60 cm. They are inserted here to cover longer distances between the optics, as they can easily be cut to the required length. As mentioned above, these distances can only be estimated, which makes the insertion of tube covers very practical. Every component mounting needs a short tube, like 5 mm length, and the covers are slipped onto them. The principle is shown in figure 4.4.

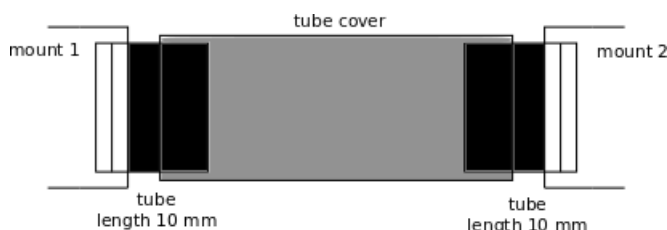


Figure 4.4: Tube covers

Variable Lens Distance Galilean Telescope The Galilean Telescope for the last expansion consists of a plano-concave lens as well as an achromatic doublet. The output beam has to be collimated, otherwise its diameter at the target would increase too much, leading to too few photons hitting the reflectors on the satellites. The beam's divergence is dependent on the distance of the two lenses. The concave lens is built in a fixed mount, so the achromat's position has to be flexible to be able to adapt the distance afterwards. As it is very difficult to set the optic into a tube at a certain and very accurate position, a solution is needed how to adjust the achromat position easier. This repeated according to the principle in 4.2. Figure 4.5 shows, that the achromat is placed into a tube with a long internal thread, which again allows to screw this tube into the other tube of the telescope construction. A retaining ring fixes the position. This way, the achromat's position simply can be changed from outside until a minimum divergence is achieved.

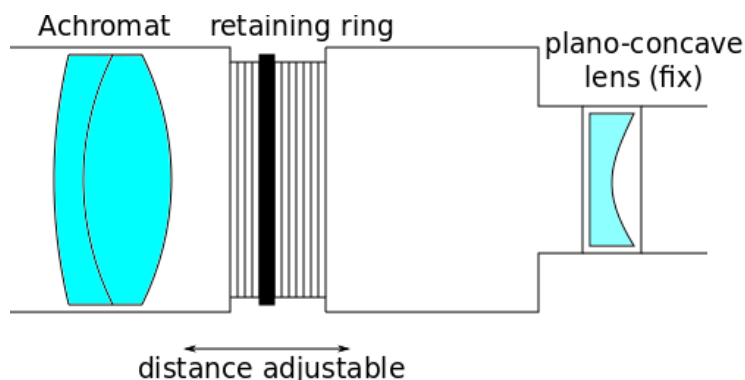


Figure 4.5: Variable lens distance, Galilean Telescope

Height-Flexible Mirror Mounting As mentioned in 4.1.1, the laser is placed on the breadboard holding the receiver channel. The beam somehow has to be lead through the overlapping part and be redirected by means of a mirror to the transmitter board. For this, two flange to thread adapters from Thorlabs are used. A hole and corresponding threads are drilled into the breadboard. The adapters can then be screwed from both sides onto the board and provide an internal SM1 thread connection where tubes can be fixed to. The mirror redirecting the beam to the optical path has to be at the height of the beam walk. This height is determined by the center height of the last lens. As the available tube lengths are standardized, it is essential to design the mirror mounting height-independently. To achieve this, an SM1 tube with 27 mm internal thread is adapted to the flange to thread adapter. Onto it, another tube (length 5 mm), fixed to a right angle kinematic mirror mount, is screwed. This allows a flexible height of the mirror mount as its position can be fixed at any height with a retaining ring. The construction is shown in figure 4.6.

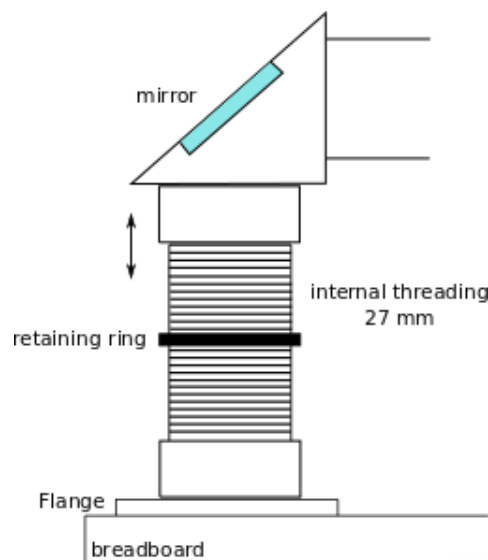


Figure 4.6: Height flexible mirror mount

Camera Fixing The camera has to be placed behind the dichroic mirror. (see 3.4). The board is not wide enough to fix the camera and its focusing lens onto it. However, it has to be directly placed behind the dichroic mirror. This mirror is put into a cage cube from Thorlabs, including SM2 external threads on each side. That is why a SM2 to SM1 adapter is used, a tube with a diameter of 1 in can be attached. In this tube the focusing lens is placed, the camera is fixed at the end of the tube, by using a SM1 to C-Mount adapter. The lens is adapted to focus the camera on infinity like the principle in paragraph "Height-Flexible Mirror Mounting" /figure 4.6. The ensemble can be seen in figure 4.7.

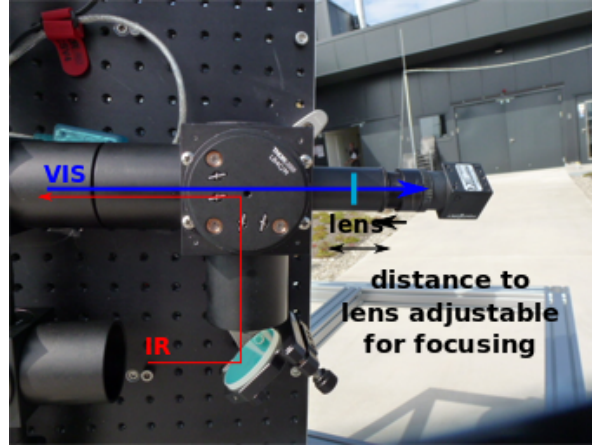


Figure 4.7: Camera fixing

Mounting of the variable beam expander The variable beam expander does not include any thread respectively tube connection. Therefore, the institute's internal workshop is asked to design and build a mounting option and threading adapters for it. The optical component has a smaller diameter on the input side than on the output side. For the input side, an aluminum cylinder with an external SM1 thread is built. Due to the expansion, a bigger tube diameter on the output is necessary. To this, also a cylinder, but with an internal SM2 thread is designed and built. Additionally, a holder is provided to stabilize the expander's position. The built-in result can be seen in figure 4.8.

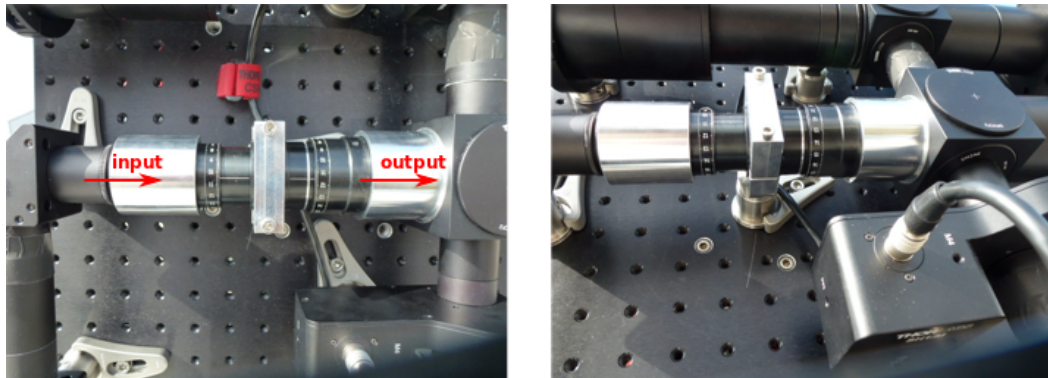


Figure 4.8: Fixing of variable beam expander

Breadboard Hole for Wires The transmitter includes some motorized parts: The filterwheel, the energy sensor, the shutter and the actuators for the movable mirror. To avoid wires at the outside of the board, possibly disturbing the mounts movement, and torsion of cables, a whole is drilled into the board through which all wires can be lead to the controlling computer. The best place for this whole can be chosen while the optics are built up.

4.3 Checking and Preparing Equipment

After receipt all optomechanics, it is checked if they all fit together to build up a coherent tube construction as planned. An important criterion for this are the right threads of adapters and adjoining tubes. Single parts like tube crossings and all mechanical designs described in section 4.2 are assembled and arranged according to the optical path in figure 4.3 to have a better overview. The optics are not implemented yet to avoid unnecessary soiling of their surfaces. Furthermore, the arrangement serves to investigate the size of the whole system and if it fits onto the breadboard. Except for some end-caps to close the tube system everything needed is assured and matches perfectly together. Also all mechanical designs fulfill their specific function.

However, building up the transmitter some components have to be prepared. First of all, the two Notch filters are mounted into the filter wheel and their positions are noted. Moreover, the camera is focused to infinity. To this, the tube assembly consisting of the lens and the camera is orientated to a target significantly far away. By screwing the tube containing the lens into the tube connected to the camera, the depiction of this target gets sharper. Eventually, at maximum sharpness, the camera is focused to infinity. Last, the magnification of the variable beam expander is adapted. The expander is investigated separately from the laser's optic add-on, otherwise the beam's diameter is too large for the sensor of the camera. The camera takes monochromatic pictures behind the variable beam expander and a python-script calculates the beam radius ($1/e^2$), similar to the proceeding in 3.2.2. The expander initially is set to a magnification of 4, referring to the data sheet. Considering 3.2.2, the magnification has to range between 3.7 and 4.5. By picking up the beam's radius without the expander, the real magnification can be verified by comparing the two radii. Some adjustment has to be done to optimize the magnification factor, then the expander is ready to be built into the transmitter.

4.4 Final System Assembly

As all optics and optomechanics are purchased, checked and prepared, the transmitter system can finally be built up on the breadboard. Since the achromat is the optic with the largest diameter in the system, its center height determines the beam walk's height above the breadboard. So first of all, the achromat is built into its 3 in tube. It is fixed with a clamp and with the smallest available post pedestal. Then threading adapters are applied temporarily. This facilitates the other mount's height adjustment. All optics are step by step first cleaned, then implemented into their mounts. Afterwards short tubes are screwed onto the mount as connections to the tube covers. Every single component's tube height is compared to the matching adapter's height applied on the achromat's tube. Deficits can be compensated by inserting post spacers. As soon as all component's mounts are set to the right height, they can be attached to the breadboard. It is helpful here to orientate to the threads in the board. This way, the components are positioned at accurate straight lines and right angles, which is essential since they are all connected via tube covers. In a last step, the tube covers are cut to their necessary lengths with a cutting tool provided by the institute's workshop. They are fixed at the junctions with a gaffa-tape. The result is a readily built-up laser transmitter, shown in figure 4.9.

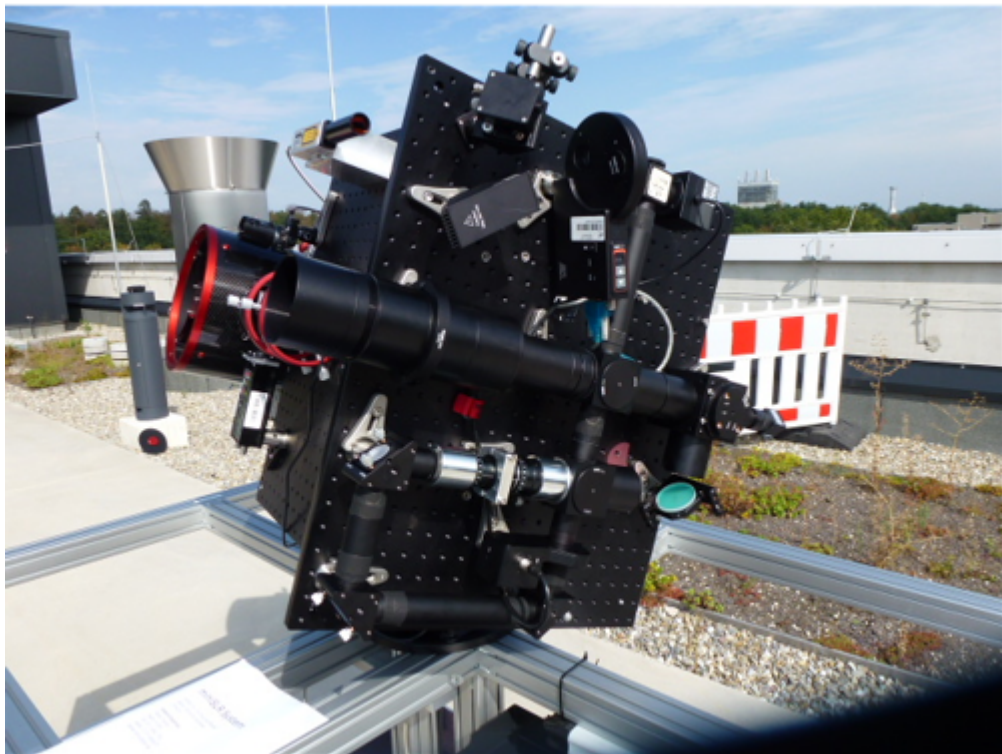
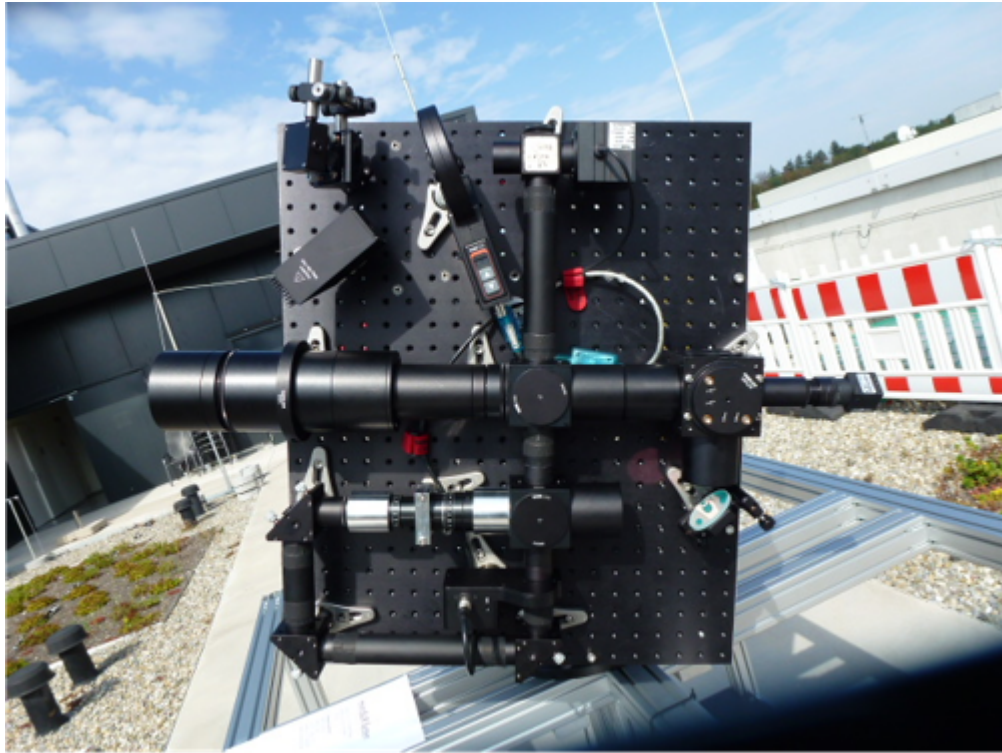


Figure 4.9: Final set-up of the laser transmitter

4.5 Beam Walk Alignment

After all components are attached to the breadboard, the beam walk has to be finely adjusted. By integrating every component into the tube system, their positions are already quite accurate, as right angles and straight lines in the path are achieved. However, fine errors can occur. Every mirror is arranged in a 45° -mount which exhibits external tip/tilt screws to change the mirror's position relative to the beam walk in very small incremental movements. By means of an infrared-viewer, the beam can be seen at the backside of the mirrors due to light scattering, allowing to adjust the previous mirror to hit the observed mirror just in its center. This procedure is done throughout every mirror, until the whole beam is visible with the infrared-viewer at the output of the system. The next task is to check the divergence of the output beam. This is done similar to 3.2.2, only using a bigger shear plate, as the beam has an approximate diameter of 6 cm. The tube containing the achromatic lens is screwed into the transmitter, finding its best position. The observed pattern after aligning is shown in figure 4.10. The beam was investigated with a shear plate directly after the provided expander (explained in subsection 3.2.2).

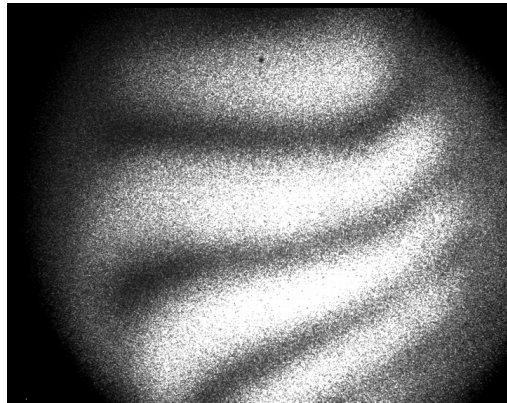


Figure 4.10: Observed pattern on Shear Plate (alignment of lens distance)

The observed pattern was almost perfect, leading to the assumption that aberrations apparent in the infrared picture are caused by the variable beam expander or the lens constellation. Nevertheless, it is the best achievable pattern. Afterwards, the system is ready to be mounted onto the miniSLR. The last required task is to connect all electrical components by wires with the operating computer. With this step the basic construction of the miniSLR is done.

5 Discussion of Further Tasks

The construction of the miniSLR's laser transmitter is now finished. The next step is to investigate its performance as it may be influenced by various factors. Still, first of all a reasonable task is to determine the real divergence of the output beam and how far it matches with the simulation with Zemax. Afterwards, the overall stability has to be considered. The miniSLR will be deployed outside. The planned housing in fact should protect the system from strong temperature variations. Nevertheless, it can not be isolated from the environment completely. For example, solar radiation may cause thermal drift of the optomechanics. The housing is made of aluminium, so temperature change may also lead to length expansion. Moreover, the transmitter is mounted onto the astronomical mount, therefore it is in motion while ranging. Additionally, the system is designed to be easily transportable. Concluding, temperature and motion may cause displacements of the optics to each other and lead to a worse divergence and also can affect the alignment of the optical axes of receiver and transmitter. It also has to be noted that turbulence in the atmosphere will influence the beam's quality additionally. That is why all those impacts have to be inspected and assessed. For example, Zemax includes a tool for tolerance analysis, intended for manufacturing defects and alignment errors. Being aware of all possible disturbances, first quality and performance measurements can be done and evaluated reliably. With everything working, the miniSLR is a very compact SLR system, can be operated fully remotely and be placed anywhere. It revolutionizes the way of SLR and opens new doors to active optical measurement possibilities.

A Appendix

A.1 nLight M30 Data Sheet

PERFORMANCE SUMMARY

Microlaser M30 Model 1039227 Driver Model 1055935
M30 S/N 721 Driver S/N 66
19 November 2015

nLIGHT

Driver Settings	Units	Value	Result	Min	Max
Drive Current	A	2.80	PASS	N/A	5.0
Drive Voltage	V	24.0	PASS	22.0	26.0

OPTICAL¹

Wavelength	nm	1064	<i>typical</i>	N/A	N/A
M ²	x DL	1.2	PASS	1.0	2.0
Waist diameter (d4σ)	μm	159	<i>typical</i>	N/A	N/A
Waist Location ²	mm	24	<i>typical</i>	N/A	N/A
Divergence (d4σ full-angle)	mrad	10	<i>typical</i>	N/A	N/A

LASER PULSE¹

Average power	W	5.6	PASS	5.3	5.7
Peak power ³	kW	38	PASS	24	N/A
Power stability, 8 hr.	%	1	PASS	N/A	10
Conversion efficiency	%	21	PASS	18	N/A
Pulse width (FWHM)	ns	5.0	PASS	4.5	7.5
Pulse Repetition Frequency (PRF)	kHz	29	PASS	25	35
Timing jitter	μs	10	<i>typical</i>	N/A	N/A

¹ All parameters at reported average power and 25°C

² Inside laser housing, measured from the output face

³ Calculated by Peak Power = 0.94 × (Average Power)/(PRF × Pulse Width)

IEC Regulation

This product is not certified in accordance with IEC 60825-1 or 21CFR1040.10/21CFR1040.11 and is solely intended to be integrated into a laser product certified by the Purchaser. The Purchaser acknowledges that their product must comply with the applicable regulations or standards before it can be sold to an end user.



WEAR LASER SAFETY EYEWEAR^{AR}

A.2 Internship Report - Lasercharacterisation nLight M30

The internship consists mainly of helping to build up and install parts of the latter two laser systems.

3 miniSLR

The miniSLR is an attempt to build up a Satellite Laser Ranging System as cheap and compact, but also as good as possible. The set-up should not be bigger than 2m x 2m x 2m. The Laser and corresponding optics (Transmit-Channel) will be placed directly on the telescope mount (red cross). Nevertheless, this is a very challenging task as the space for optics is limited. The corresponding Laser is investigated in the Internship.

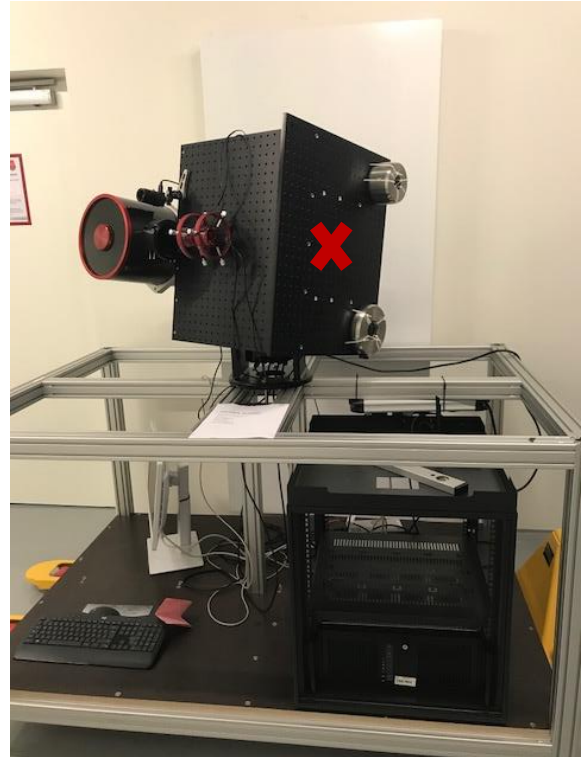


Figure 1 miniSLR

3.1 Laser characterization

In the beginning of the internship, various lasers should be characterized for a better evaluation of the lasers' behavior.

In the case of the miniSLR, this is the Laser nLight M30 from manufacturer nLight. The Laser is a diode pumped passively q-switched solid state Laser (DPSS) with an emitting wavelength of 1064 nm. According to the data sheet, the average power comes to 5.6 W. The Laser is mounted on a steel rostrum so that heat can be diverted. Its signal comes from an external pulse generator.

The beam quality factor M^2 is measured, the pulse width, the beam stability and the stability of the beam radius are taken.

M^2

For the determination of the value of M^2 the beam radius is measured at certain distances around the beam waist. For this an artificial beam waist is created with a plano-convex lens (the “real” waste of the laser is inside the housing thus no measurement is possible) which is hung up on rails and can be moved. Various monochromatic pictures are taken with a camera with a CMOS-Sensor behind this lens around the beam’s waist.

Following Figure shows the Construction:

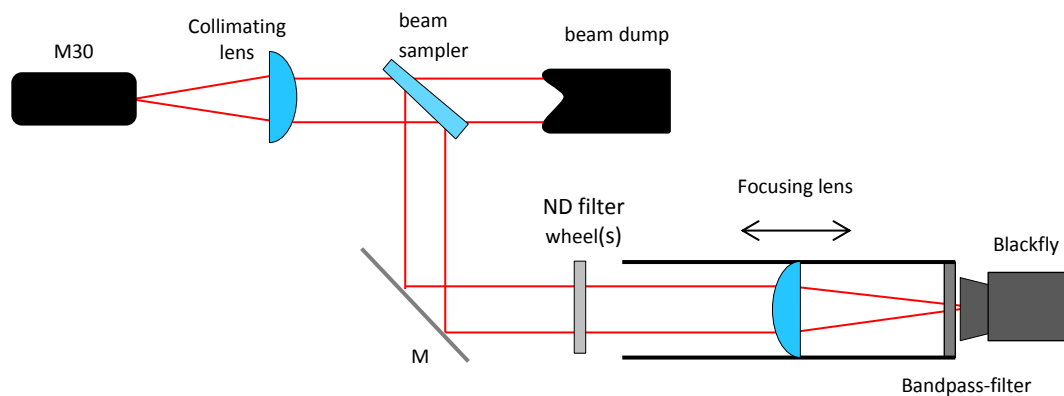


Figure 2 Construction M^2 -Measurement

After collimating the beam with a plano-convex Lens ($f = 150$ mm) a beam sampler couples out about 94 % of the beam Energy and steers it into a beam dump. This was done to save some optics as their damage threshold is under the Laser’s Intensity. Following, there are some Neutral-Density Filters that again moderate the beam’s intensity. Without them the pixels of the camera would be oversaturated and the image analysis would be incorrect. The focusing lens creates the artificial beam waist as mentioned before until the beam eventually steers onto the sensor of the camera. The camera is connected via USB 3.0 to a computer with the matching software installed to pick up the pictures.

To get the value of M^2 a python script is written which finds the beam in the picture, performs a Gaussian fit and calculates the beam radii in x- and y-direction. The squared beam diameters are applied over distance z (from the lens to the CMOS-Sensor) and a polynom of second order is fit in (Figure 3). By means of the Coefficients of this polynom fit the value of M^2 can finally be calculated.

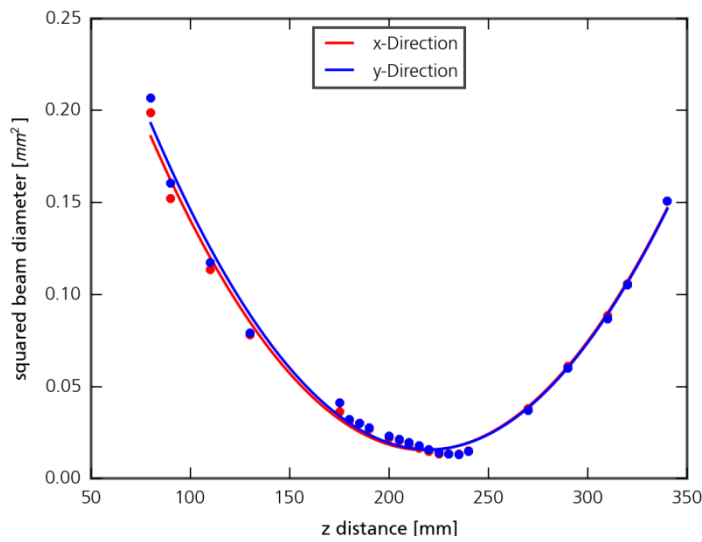


Figure 3 Polynomfit M^2 , nLight M30

	M^2
x	1.1
y	1.2

Pulse width (FWHM)

To measure the pulse shape a photodiode with a maximum input Voltage of 2V is used. To avoid oversteering, a beam sampler with a Reflectivity of 4 % was placed into the path. The reflection is detected by the diode connected to an oscilloscope and the data of the wave form can easily be saved on an external storage medium. It is plotted and pulse width is measured with a self-written python script.

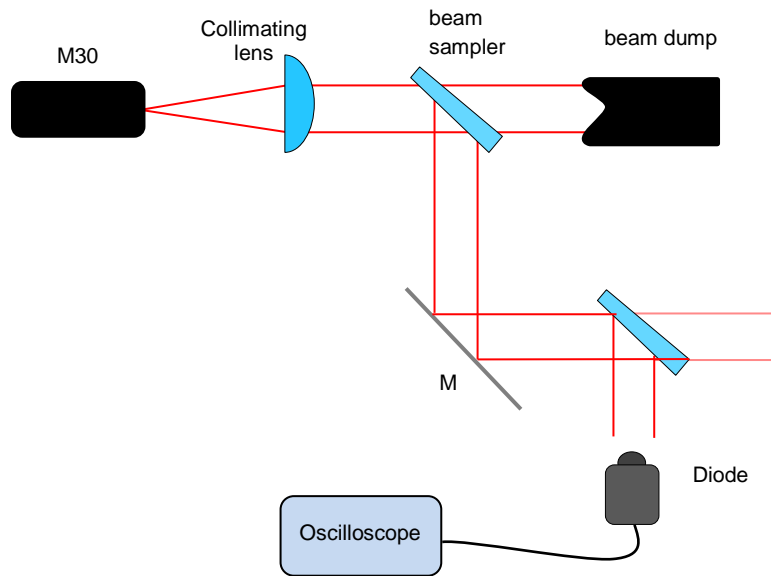
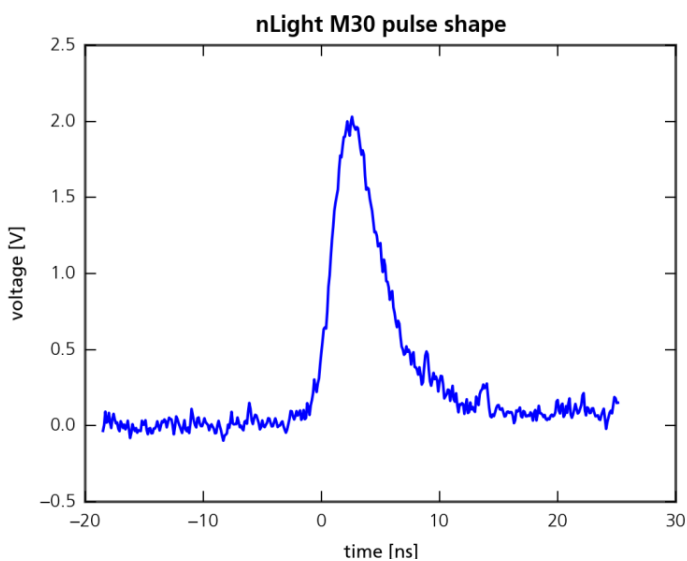


Figure 4 Construction pulse Measurement



	Pulse width (FWHM)
Reference value (data sheet)	5.0 ns
Measured value	4.3 ns

Figure 5 pulse shape, nLight M30

Beam stability

As this laser will have to shoot at certain targets in space, it is important to have a clue about the beam stability, i.e. whether and how strong the laser beam staggers around in the cross-section plane (angular). With this information one can estimate and explain possible measuring mistakes.

The construction is similar to the one used for M^2 -Measurement. The camera is focused on infinity with a plano-convex lens, the focusing lens ($f = 200 \text{ mm}$) is used to investigate the far field of the beam. The beam waist position is applied to the sensor of the camera.

Again a python script is written, which is connected to the CMOS-Camera used before. The script automatically takes pictures, analyzes them and calculates the angle deviation in x (phi) and y (teta). It delivers three different plots: phi over time, teta over time, teta over phi.

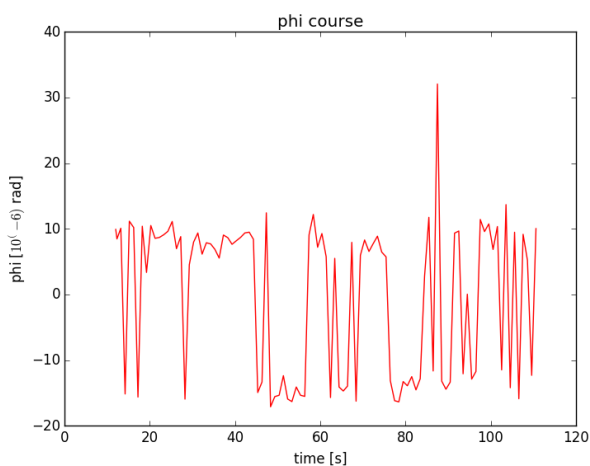


Figure 8 angle deviation phi (x) over time

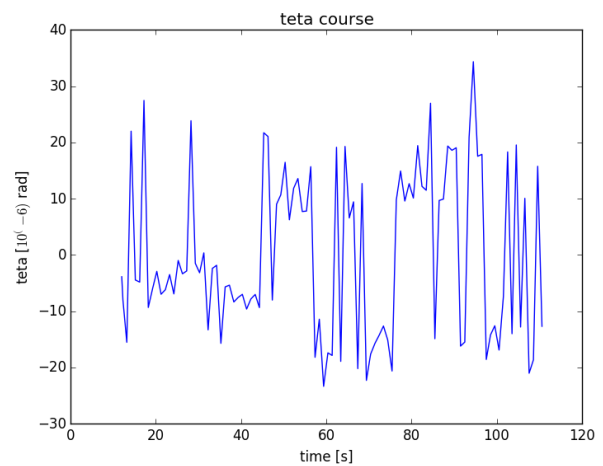


Figure 8 angle deviation teta (y) over time

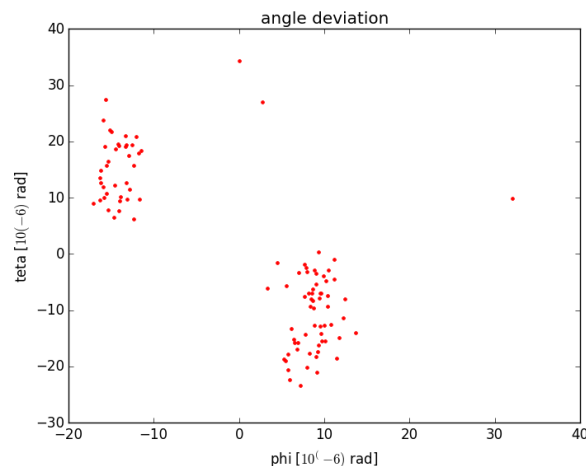


Figure 8 teta over phi

Beam Radius

During the described measurement one could notice a little instability of the beam radius. So another python script is written that takes a picture of the beam about every ten minutes, calculates the radius and eventually plots the radii over time. The radius in x-direction is marked with red, the radius in y-direction with blue. The script was executed for about 4 hours and there was a relative change of only about 10%.

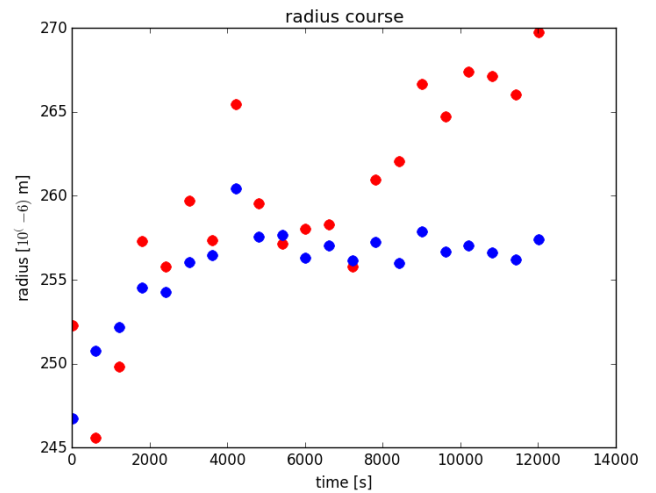


Figure 9 beam radius course, nLight M30

References

- [1] International Laser Ranging Service. ILRS Overview. <https://ilrs.cddis.eosdis.nasa.gov/about/Overview.html> [Online; accessed 20-December-2018]
- [2] L. Humbert, T. Hasenohr et al. *Design and commissioning of a transportable laser ranging station STAR-C*. Advanced Maui Optical and Space Surveillance Technologies Conference, Maui, 2017
- [3] G. Kirchner, F. Koidl et al. *Laser measurements to space debris from Graz SLR station*. Advances in Space Research, Volume 51, Issue 1, 2013, Pages 21-24, ISSN 0273-1177
- [4] M.R. Pearlman, J.J. Degnan et al. *The International Laser Ranging Service*. Advances in Space Research, Vol. 30, No. 2, pp. 135-143, July 2002, DOI:10.1016/S0273-1177(02)00277-6
- [5] D. Hampf, F. Sproll et al. *First successfull satellite laser ranging with a fibre-based transmitter* German Aerospace Center, Institute of Technical Physics, Stuttgart, 2016
- [6] D. Hampf, P. Wagner, P. Luetzen et al. *MiniSLR: A fully automated miniature satellite laser ranging ground station*. International Astronautical Congress, IAC-18.B6.1.8x42690, Bremen, 2018
- [7] H. Krag, S. J. Setty et al. *Ground-Based Laser for Tracking and Remediation – An Architectural View*. International Astronautical Congress, IAC-18-A6.7.1, Bremen, 2018
- [8] T. Hasenohr, L. Humbert et al. *STAR-C: Towards a transportable Laser Ranging Station* International Astronautical Congress, IAC-17,A6,IP,5,x37746, Adelaide, 2017
- [9] M. Pearlman, C. Noll. *A view of ILRS station perfomance*. ILRS Technical Workshop, Riga, 2017
- [10] D. Hampf, F. Sproll, T. Hasenohr. *OOOS: a hardware-independent SLR control system*. ILRS Technical Workshop, Riga, 2017
- [11] D. Hampf, L. Humbert et al. *Kosmische Müllhalde* in Physik Journal, Weinheim: Wiley - VCH Verlag GmbH & Co. KGaA, January 2018
- [12] F. K. Kneubühl, M. W. Sigrist. *Laser; 7. Auflage*. Wiesbaden: Vieweg + Teubner, GWV Fachverlage GmbH, 2008
- [13] T. Graf. *Laser - Grundlagen der Laserstrahlungsquellen* Wiesbaden: Vieweg + Teubner, GWV Fachverlage GmbH, 2009

- [14] D. Meschede. *Optics Light and Lasers - The Practical Approach to Modern Aspects of Photonics and Laser Physics; Third Revised and Enlarged Edition*. Weinheim: Wiley - VCH Verlag GmbH & Co. KGaA, 2017
- [15] E. Hering, R. Martin (ed.) et al. *Optik für Ingenieure und Naturwissenschaftler - Grundlagen und Anwendungen*. München: Carl Hanser Verlag, 2017
- [16] C. Gerhard. *Tutorium Optik - Ein verständlicher Überblick für Physiker, Ingenieure und Techniker*. Berlin, Heidelberg: Springer-Verlag, 2016
- [17] Ophir Photonics. Ophiropt.com - Ophir Photonics Blog Laser Measurement. <https://www.ophiropt.com/blog/laser-measurement/laser-peak-power-and-average-power-whats-the-difference/> [Online, accessed 16-February-2019]
- [18] OR Laser. Or-laser.com - News zu OR Laser. <https://www.or-laser.com/de/news/kleiner-exkurs-kenngrößen-eines-lasersystems/> [Online, accessed 16-February-2019]
- [19] Qioptiq. Qioptiq.de - Variable Strahlaufweitung. <https://www.qioptiq-shop.com/Praezisionsoptik/LINOS-Laseroptik/LINOS-Variable-Strahl-Aufweitungs-systeme/Variable-Strahlaufweitungen.html> [Online; accessed 30-November-2018]
- [20] Thorlabs. Thorlabs.de - Thermal Power Sensors (C-Series). https://www.thorlabs.de/newgrouppage9.cfm?objectgroup_id=3333&pn=S370C [Online; accessed 30-November-2018]
- [21] Thorlabs. Thorlabs.de - Free-Space Biased Detectors. https://www.thorlabs.com/newgrouppage9.cfm?objectgroup_id=1295&pn=DET10C2 [Online; accessed 30-November-2018]
- [22] Thorlabs. Thorlabs.de - Shortpass Dichroic Mirrors/Beamsplitters. https://www.thorlabs.de/newgrouppage9.cfm?objectgroup_id=9240&pn=DMSP805L#5306 [Online; accessed 01-December-2018]
- [23] Thorlabs. Thorlabs.de - Shearing Interferometers. https://www.thorlabs.de/newgrouppage9.cfm?objectgroup_id=2970 [Online; accessed 12-December-2018]
- [24] Edmund Optics. Edmundoptics.de - Optische Filter. <https://www.edmundoptics.de/resources/application-notes/optics/optical-filters/> [Online; accessed 01-December-2018]
- [25] Edmund Optics. Edmundoptics.de - Notchfilter. <https://www.edmundoptics.de/p/1064nm-25mm-diameter-od-4-notch-filter/21660/> [Online; accessed 01-December-2018]
- [26] University of California San Diego - Ultrafast and Nanoscale Optics Group - M. E. Riley, M. A. Gusinow - *Laser beam divergence utilizing a lateral shearing interferometer*. http://emerald.ucsd.edu/Teaching/ECE181/ECE181_

files/Lateral%20Shearing%20Interferometer%20paper.pdf [Online; accessed 12-December-2018]